PRELIMINARY STUDY ON MEDIUM FORMAT CAMERAS COMPARISON VIA PHOTO RESPONSE NON-UNIFORMITY

by

EDGAR FRITZ

B.A., University of California, San Diego, 2001

A thesis submitted to the

Faculty of the Graduate School of the

University of Colorado in partial fulfillment

of the requirements for the degree of

Master of Science

Recording Arts Program

2019

This thesis for the Master of Science degree by

Edgar Fritz

has been approved for the

Recording Arts Program

by

Catalin Grigoras, Chair

Jeff M. Smith

Carol Golemboski

Date: December 14, 2019

Fritz, Edgar (M.S., Recording Arts Program)

Preliminary Study on Medium Format Cameras Comparison Via Photo Response Non-Uniformity

Thesis directed by Associate Professor Catalin Grigoras

ABSTRACT

This is a preliminary study on Medium Format cameras. This study utilizes Photo Response Non-Uniformity (PRNU), which is part of the background noise inherent in all digital camera sensors, to compare between Medium Format cameras of the same make and model. PRNU is comprised of tiny imperfections at the pixel level and is sometimes referred to as the camera's "fingerprint." This background noise can be extracted and utilized to compare between a reference image and a source camera. Two different methods of PRNU extraction were utilized in this study, a Gaussian method, and a Wiener method. The inter-variability and intra-variability between a reference image and sets of natural scene images was used to compare cameras.

The form and content of this abstract are approved. I recommend its publication.

Approved: Catalin Grigoras

To my wife and kids, for always encouraging me to reach my goals.

ACKNOWLEDGEMENTS

Thank you to my professors at the University of Colorado Denver.

TABLE OF CONTENTS

LIST OF FIGURES

FIGURE

LIST OF TABLES

TABLE

CHAPTER I

DIGITAL PHOTOGRAPHY BACKGROUND

Modern digital cameras are ubiquitous in our society today. The digital revolution transformed photography forever. Digital photography eliminated the wait of developing and printing images before confirming if you even captured the shot. It brought users instant feedback and the ability to review images wherever they were. But digital cameras brought much more than that, they include a wealth of information never before captured in the film era. Digital images contain data embedded within the file. This is called the metadata, and it contains valuable information that can be invaluable from a forensic standpoint. Embedded within the file you may find information about when the image was taken, the make, model, and serial number of the camera, geolocation, camera settings, lens information, and even if an image has been edited after it was captured. Information not only can be obtained from the file's metadata, but the images themselves can be analyzed and inferences can be made from them. Digital images can be used forensically to identify locations from elements within the image, dates and times from shadows, subject identification from biometrics, size of objects from known objects comparison, and many more. You can even ascertain which camera took an image from the inherent background noise of a digital sensor. Today, you'd be hard pressed to find someone without some sort of image capturing device on them at all times. Digital images can be the one piece of corroborating evidence that ties together an entire court case. They are a big part of today's criminal justice system, that is why forensic scientists have been studying their properties since the dawn of the digital age.

Digital Noise

A digital camera works by allowing light to enter though an opening in an optical lens (aperture) for a specified length of time (shutter speed). The photons of light that enter are focused on a digital sensor which is made up of an array of pixels. Each pixel is made of a photosensitive material responsible for gathering photons of a specific wavelength of light. Photons captured by the

photosensitive part of a pixel stimulate the emission of electrons, one for each captured photo. The accumulated photoelectrons are counted and proportionally converted to a voltage. That number can then be amplified depending on the sensitivity to light set on the camera (ISO setting). This voltage is then digitized in an analog to digital converter (ADC) and converted into 1s and 0s to be written out to a file. This binary code can be thought of as the RAW image data. Additional information will be written to the file by the camera as metadata for future decoding of the image.

The process described above would be an ideal camera with ideal components and processes. But no camera can perform to the ideal, hence no image is an exact representation of the photons that struck the sensor. All digital images will possess some inherent noise, which comes from several sources during the image acquisition process. Noise can be thought of as variations in color or intensity from what the true scene was. This noise can be grouped into two general types: Random Noise, and Fixed Pattern Noise.

Each electronic circuit in the signal processing chain suffers from random fluctuations. These fluctuations can come from the photosensitive components of the sensor, the ISO gain, and/or the ADC digitization. Horizontal and Vertical Banding Noise (HVBN) is an example of random noise in the image capturing process. HVBN manifests itself as linear color and intensity fluctuations in the rows or columns and look like bright bands in the image. HVBN noise can be caused by errors in the sensor readout; that is when rows of pixels are activated and readout down the pipeline. ISO settings will also introduce HVBN as the ISO is increased. ISO is a scalar multiplier of the photoelectron count, so higher settings will amplify errors. ADC digitization can introduce HVBN noise with errors in the digital conversion process (1). There are several other sources of random noise that can affect a digital image.

Fixed Pattern Noise is a pattern that will be stamped in all images from the same sensor under the same conditions. There are many factors that will contribute to Fixed Pattern Noise at different stages of the image capturing process. Thermal agitation of electrons in the photoreceptors of a sensor

can liberate some electrons. These freed electrons will be counted as if they were photons that were present in the image and will be added to the RAW data. Thermal electrons are freed at a relatively constant rate creating constant imperfections in an image. Thermal Noise will increase with exposure time and will show up as "hot pixels" in an image. These hot pixels are overexposed pixels that will show up in the same spot repeatedly.

Pixel Non-Uniformity is a general term for the imperfections in the micron sized pixels of a sensor, it is comprised of two types. Dark Signal Non-Uniformity (DSNU) is the offset from the average across the sensor at a particular temperature and integration time without external illumination. Basically, this noise is found when an image is taken in complete darkness. DSNU will be fixed in all images taken in total darkness. Pixel Non-Uniformity is also found in illuminated pixels. Pixels have acceptable levels of variation in capturing efficiency, photon counting accuracy; variations in pixel size, shape, and substrate material. Not all pixels in a sensor are made the same, these tiny variations are called the Photo Response Non-Uniformity (PRNU). PRNU comes from the gain or ratio between optical power on a pixel versus the electrical signal output. When the photoreceptive cells in a sensor are illuminated evenly, each cell should ideally output the same voltage, but they don't. PRNU will be ingrained in all images as part of the background noise and will be an ever-present fixed pattern. That is why PRNU is often referred to as the camera's "fingerprint." PRNU noise grows in direct proportion to the exposure level, so brighter pixels will show more PRNU noise. PRNU noise will be reproduced for all images taken under the same conditions and settings (2).

Photo Response Non-Uniformity

PRNU can be used for several forensic methods. One example is to test for the presence of a specific PRNU in an image, which can achieve reliable device identification (prove that a certain camera took a given image). PRNU can also help prove two images were taken by the same device (device linking). The presence of PRNU is indicative of the fact that the image is natural and not a computer

rendering. By establishing the absence of the PRNU in individual image regions, it is possible to discover maliciously forgery attempts. By detecting the strength or form of the PRNU, it is possible to reconstruct some of the processing that was done to an image. PRNU is used as a template to estimate geometrical processing, such as scaling, cropping, or rotation. Non-geometrical operations are also going to influence the strength of the PRNU in the image and thus can be potentially detected. The spectral and spatial characteristics of the PRNU can be used to identify the camera model or distinguish between a scan and a digital camera image (the scan will exhibit spatial anisotropy) (3).

PRNU and the Daubert Standard for Evidence Admissibility

PRNU has proven to be extremely valuable as a forensic tool. During the court proceedings of the United States of America v. Nathan Allen Railey, United States Court of Appeals for the Southern District of Alabama, prosecutors showed child pornography images in question were created by the defendant's camera by comparing the PRNU. This identification was challenged in an admissibility hearing to verify the technology met the Daubert standard. It met the challenge as follows (4):

Whether the theory or technique employed is generally accepted in the scientific community: PRNU source camera identification was first introduced in 2005 by Lukas, Fridrich, and Goljan, where they detailed how to determine a digital image's origin using sensor pattern noise (5). Numerous papers have subsequently been written expanding on these methods and techniques.

Whether the technique has been subjected to peer review or publications: There have been numerous peer-reviewed publications on the subject appearing in such periodicals as IEEE, SPIE, the International Conference on Image Processing, EURASIP Journal on Image and Video Processing, International Conference on Computer Science and its Applications, etc.

Whether the technique has been tested or can be tested: There exist many techniques for PRNU extraction and comparison. These methods and algorithms are tested and peer reviewed as they

are developed. Validation is a typical part of the scientific process, and some validation has been conducted by the Law Enforcement Analysis Facility, an independent testing company in NY (6).

Whether an error rate can be determined: There have been several large-scale tests conducted to test identification error and false positive rates. One such study was conducted by Miroslav Goljan on more than a million images. It tested PRNU image identification via peak to correlation energy, with a false positive rate at less than .00024% , and the false rejection rate at less than .0238% (7).

PRNU met the Daubert standard in this court case, and expert testimony regarding PRNU implementation was admitted into court. US v Railey provided support for future PRNU implementation against Daubert challenges since the theory or technique employed met the standards set and is generally accepted in the scientific community as a valid method.

Prior Research

Camera identification has been studied extensively for decades now. Researchers have found several ways of matching images with the camera that produced them. A variety of features have been employed, including color filter array design, pixel color value interpolation algorithm, image sensor anomalies, lens characteristics and anomalies, and image processing pipeline characteristics (8).

PRNU extraction for camera comparison has also been widely studied. There have been various attempts to improve the accuracy of digital camera identification. Several approaches aim to achieve this by improving the estimate of PRNU. Some apply Maximum Likelihood Estimation (MLE) for estimation of a multiplicative factor from reference images (9). Other research suppresses unwanted artifacts from sensor pattern noise. This is achieved by preprocessing the PRNU by subtracting Zero Mean and applying Wiener filtering (10). Some research proposes extracting PRNU per color channel in a Color Decoupled PRNU extraction method (11). The effect of denoising filter has been investigated using sparse 3D transform-domain collaborative filtering for more accurate noise extraction (12). Another documented method uses edge adaptive PRNU predictor context adaptive interpolation (13,

14). Another technique is to pre-process the estimated PRNU for removal of non-unique artifacts. These techniques work by identifying and suppressing the peaks according to local characteristics in the magnitude spectrum of the reference PRNU with spectrum equalization, improving the detection accuracy further (15). Furthermore, other methods improve performance by using better statistical detection. Some use peak to correlation energy to attenuate hidden periodic patterns (16). Others use correlation over circular cross-correlation norm to further decrease the false-positive rate (14).

Though there are several methods and techniques that explore source camera identification via PRNU comparison, few use RAW image data to achieve this. Those that do use RAW data only focus on either identification of source device of the same model, or different devices of the same model but not different models or cameras (17). If you browse through PRNU publications, you will find researchers typically utilize JPEG compressed images from mass manufactured consumer level cameras. The sensor quality and size used in typical research overlooks the best available sensors in the market today. One paper tried to specifically address this issue but only obtained data from "mid-end and high-end popular consumer digital cameras"(18), not take into consideration professional level medium format cameras. Below is a cross sample of typical cameras utilized in PRNU literature:

Table 1 Cross Sample of Typical Cameras and Specifications

Make	Model	Sensor Type	Sensor Size	Sensor Resolution	Pixel Area	Mega Pixels	File Format
Nokia	6600	Cell Phone	Not Provided	640 x 480	Not Provided	.3 MP	JPEG 8 bit
Canon	PowerShot A430	CCD	4.8 x 3.6 mm	2272 x 1704	4.33 μm^2	4.1 MP	JPEG 8 bit
FUJIFILM	FinePix J50	CCD	5.75 x 4.32 mm	3264 x 2448	3.03 μm^2	8.2 MP	JPEG 8 bit
Olympus	MJU 7050	CCD	6.16 x 4.62 mm	4315 x 3244	2.04 μm^2	14 MP	JPEG 8 bit
Casio	EX-Z150	CCD	5.75 x 4.32 mm	3264 x 2448	2.99 μm^2	8.29 MP	JPEG 8 bit
Canon	EOS 60D	CMOS	22.3 x 14.9 mm	5196 x 3464	18.4 μm^2	18 MP	RAW 14 bit C2R

Medium Format Sensors

We have discussed how PRNU has been studied by numerous people with various methods and under various conditions for accuracy, and robustness, but no research has been conducted on the top quality sensors in the market. The objective of this thesis is to look beyond consumer level cameras and study professional level medium format cameras. Medium format refers to any sensor larger than a full frame DSLR (or the traditional 35mm sensor at 24 x 36mm). The advantage of medium format sensors comes not just from their size, but from the larger pixel area, and meticulously calibrated sensors. Medium format sensors provide a wider dynamic color range, larger field of view, and shallower depth of field. Larger pixels have more light-gathering capability. Finer and more detailed tonal information can be produced, delivering more information in the final file. But more importantly for camera comparison, better build, quality control, and smaller production scale.

This thesis focuses specifically on today's top end medium format camera manufacturers, FUJIFILM, Hasselblad, and Phase One. The following cameras were used in this research as being recent top end cameras from said manufacturers: FUJIFILM GFX 50S with a 50MP sensor, FUJIFILM GFX 100 with a 100MP sensor; Hasselblad H6D 100c camera with a 100MP sensor, Hasselblad X1DII-50c mirrorless camera with a 50MP sensor; Phase One IQ3 with a 101MP sensor, Phase One IQ4 with a 151MP sensor. Medium format sensors provide much larger images with better resolution and more mega pixels than any sensor found in prior studies into PRNU. The Pixel Area (size of each pixel) is also much larger allowing for greater light gathering capability. And the RAW recording allows for 14 and even 16 bits of depth yielding millions of more colors, that is 1.6×10^7 for an 8 bit image vs. 2.8×10^{14} for a 16 bit image. The following table shows the specifications for the cameras used in this study.

Table 2 Medium Format Sensors Included in this Study and their Specifications

Make	Model	Sensor Type	Sensor Size	Sensor Resolution	Pixel Area	Mega Pixels	File Format
FUJIFILM	GFX 50S	CMOS	43.8mm x 32.9mm	8256 x 6192	28.2 μm^2	51.4 MP	RAW 14 bit RAF
FUJIFILM	GFX 100	CMOS BSI	43.8mm x 32.9mm	11648 x 8736	14.14 μm^2	101.9 MP	RAW 16 bit RAF
Hasselblad	X1DII-50c	CMOS	43.8 x 32.9mm	8272 x 6200	27.98 μm^2	51.3 MP	RAW 16 bit 3FR
Hasselblad	H6D-100c	CMOS	53.4 x 40.0 mm	11600 x 8700	21.16 μm^2	100 MP	RAW 16 bit 3FR
Phase One	IQ3-100MP	CMOS	53.7 x 40.4mm	11608 x 8708	21.44 μm^2	101.1 MP	RAW 16 bit IIQ
Phase One	IQ4-150MP	CMOS BSI	53.4 x 40.0mm	14204 x 10652	14.14 μm^2	151 MP	RAW 16 bit IIQ

Here is what the manufacturers have to say about their cameras.

The FUJIFILM GFX 50S features a 43.8×32.9mm CMOS medium format sensor, boasting an effective resolution of 51.4 million pixels. The FUJIFILM GFX 100 pairs a newly-developed back-illuminated 102MP imaging sensor with a blazingly fast X Processor 4 processing engine to create a combination capable of outputting 16-bit images with amazing color fidelity, rich shadow detail, and incredible dynamic range. Its back-illuminated structure enhances image quality by bringing the exposure plane closer to the color filter array. Sharpness is also enhanced, while moiré and false colors are near eliminated through the omission of an optical low-pass filter (19).

Figure 1 FUJIFILM Sensor Size Comparison

Hasselblad camera sensors are individually calibrated to ensure maximum performance in any given situation. A massive amount of data is gathered for each unit in the production stage in order to study the variations that can occur and see how the sensor performs under different circumstances. Through Hasselblad's rigorous sensor testing, all irregularities are corrected automatically when shooting with any Hasselblad camera (20).

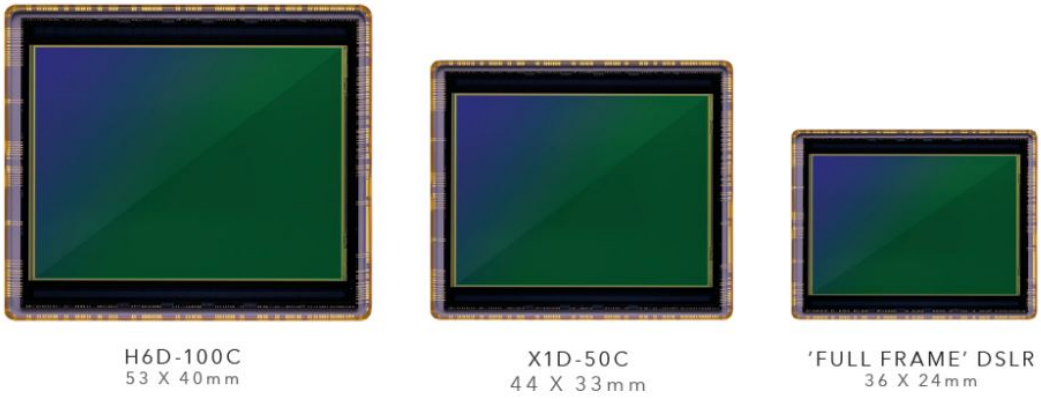

Figure 2 Hasselblad Sensor Size Comparison

The full frame medium format sensors found in the Phase One IQ Digital Backs are 2.5x larger than that of full frame DSLR cameras, and 1.5x larger than cropped sensor mirrorless medium format. The use of a larger sensor means more light, and therefore more information is available when converting captured light into a digital file. The availability of more data allows Phase One to honor the quality of that data, translating to more efficient use of information and less interpolation (21).

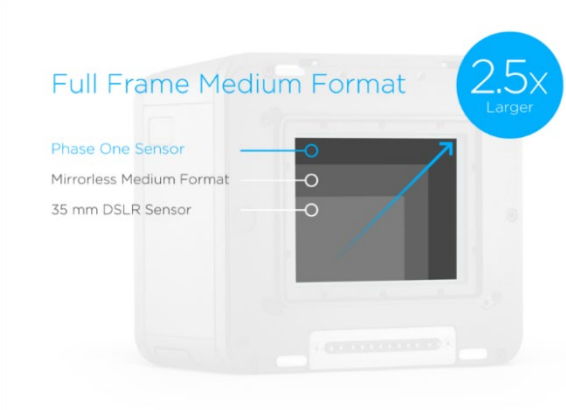

Figure 3 Phase One Sensor Size Comparison

CHAPTER II

CAMERA FINGERPRINT

Materials and Methods

Flat field (evenly illuminated neutral wall) images were collected from each camera. The images were slightly underexposed, so no pixels maxed out their threshold. A few natural scene images were also collected for comparative analysis. In order to obtain the full quality of each sensor, RAW images were collected. RAW images would avoid the undesired addition of JPEG artifacts into the background noise. In-camera noise reduction was not applied to any of the images collected to maintain proper PRNU signatures. ISO 100 was used for all images collected to limit random noise. All calculations were performed on a Windows 10, 64-bit operating system with Intel Core 17-8550U CPU at 2.0 GHz and 16.0 GB of RAM. Matlab R2019b version 9.7.0 build 1190202 was utilized for all computations.

RAW files were converted into uncompressed TIFF files in Adobe Bridge CC 2019 v9.1.0.338 with Adobe Photoshop CC 2019 v 20.0.7 for the Hasselblad and FUJIFILM cameras. The Image Processor tool converted folders of RAW images into uncompressed TIFF files. Note this process does not provide bit depth options and automatically converted the images into 8 bits per channel. Phase One images were processed using Capture One Pro v12.1.1.19 since Adobe does not support IIQ file format. The Process Recipe tool was used in Capture One to convert RAW images into uncompressed TIFF files. This process does allow for 16 bit TIFF conversion, but files were converted to 8 bits per channel for consistency.

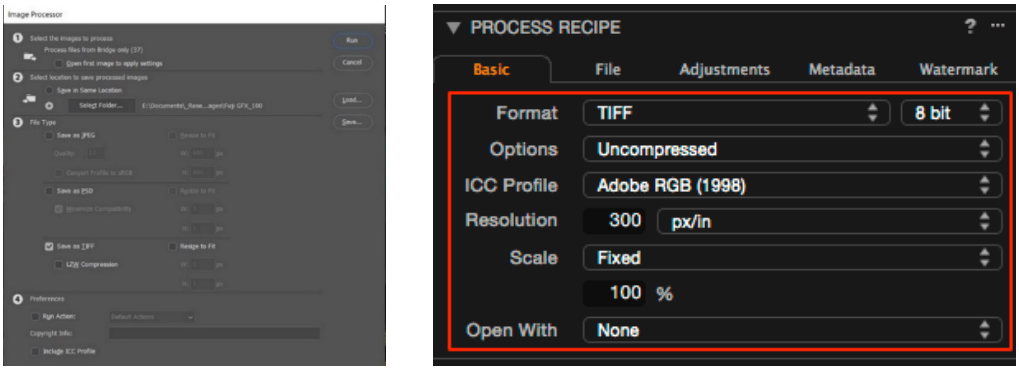

Figure 4 RAW to TIFF Conversion

PRNU Suitability Test

Once the images were converted to TIFF files, they were tested for PRNU suitability with a denoising filter prior to PRNU extraction. The Wavelet method was uses to denoise the images. This is a spatial adaptive statistical model for wavelet image coefficients as zero-mean Gaussian random variables with high local correlation. This method assumes a marginal prior distribution on wavelet coefficients variances and estimates them using an approximate maximum a posteriori probability rule. Then an approximate minimum mean squared error estimation procedure was applied to restore the noisy wavelet image coefficients (22). Simply put, the wavelet method analyses data at a local level as well as at a global level. The result tells us if the images in question are suitable for PRNU extraction.

The flat field reference images collected were tested with a Wiener method for suitability of PRNU extraction. The following figures show each set of images and the cross correlation of the intra/inter-variability. This process plots the first image in the set as the evidence and compares the inter-variability (the variation within each file), and the intra-variability (the variation between all the files), and calculates the cross correlation amongst them for PRNU suitability. Note some reference flat field image sets were reduced to 20 images for computational considerations. All reference flat field image sets were found to be suitable for PRNU analysis.

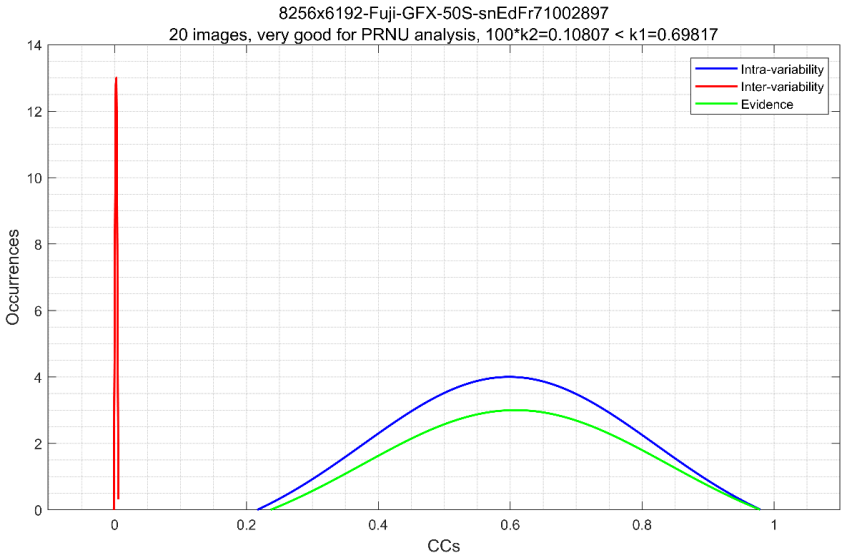

Figure 5 FUJIFILM GFX 50s PRNU Suitability Test

Computes CC1, CC2...

ans =

0.0011 0.6982

0.0004 0.7434

20 images, very good for PRNU analysis, 100*k2=0.10807 < k1=0.69817

8256x6192-Fuji-GFX-50S-snEdFr71002897

Figure 5 Continued

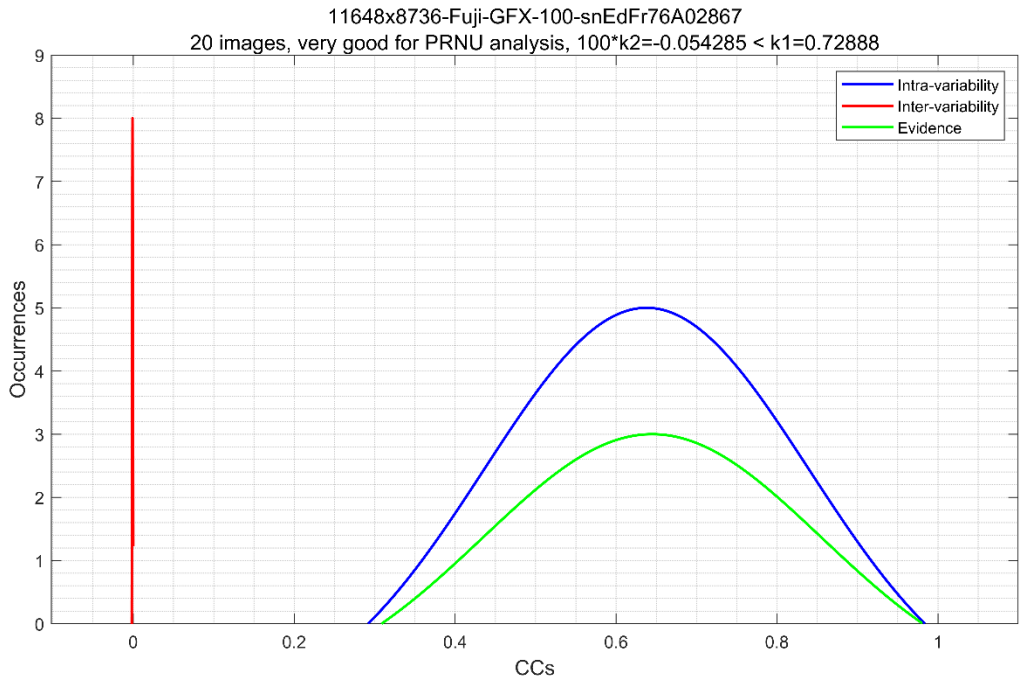

Computes CC1, CC2...

ans =

-0.0005 0.7289

-0.0003 0.7695

20 images, very good for PRNU analysis, 100*k2=-0.054285 < k1=0.72888

11648x8736-Fuji-GFX-100-snEdFr76A02867

Figure 6 FUJIFILM GFX 100 PRNU Suitability Test

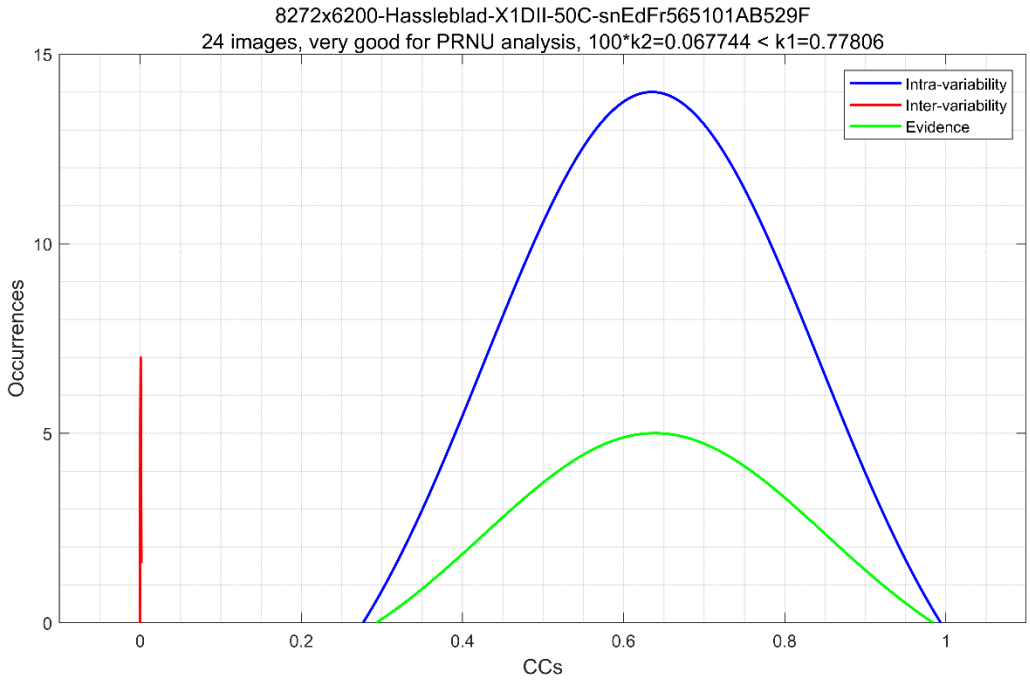


```
Computes CC1, CC2...

ans =

   0.0007    0.7781

   0.0011    0.8505

24 images, very good for PRNU analysis, 100*k2=0.067744 < k1=0.77806

--------------------------------------------------------------------------------

8272x6200-Hassleblad-X1DII-50C-snEdFr565101AB529F
```

Figure 7 Hasselblad X1DII 50c PRNU Suitability Test

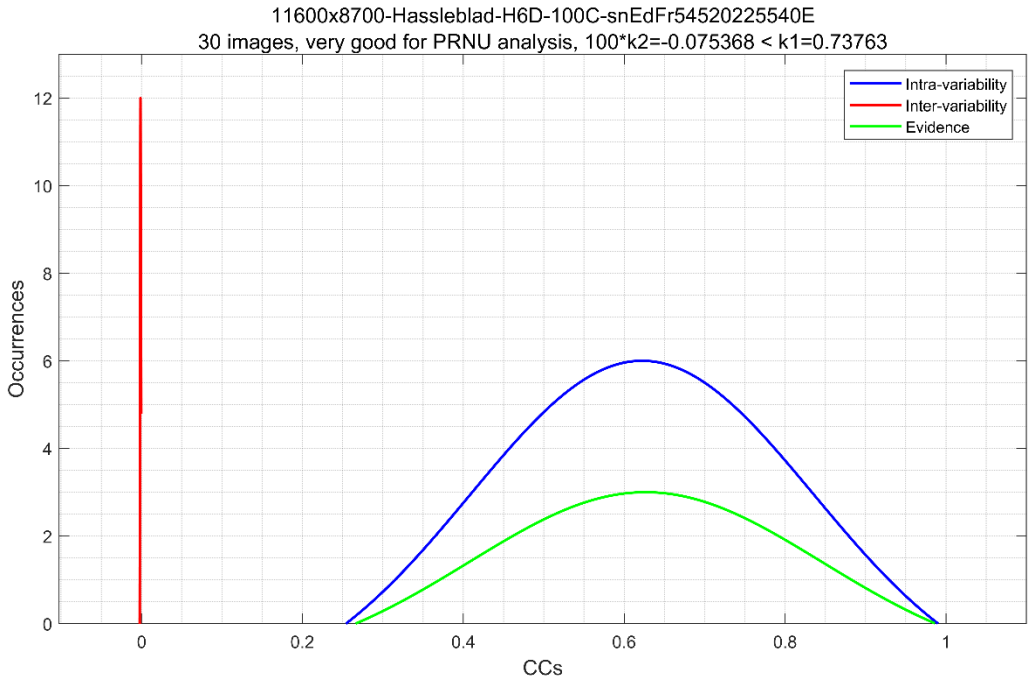


```
Computes CC1, CC2...

ans =

   -0.0008    0.7376

   -0.0008    0.7840

30 images, very good for PRNU analysis, 100*k2=-0.075368 < k1=0.73763

--------------------------------------------------------------------------------

11600x8700-Hassleblad-H6D-100C-snEdFr54520225540E
```

Figure 8 Hasselblad H6D 100c PRNU Suitability Test

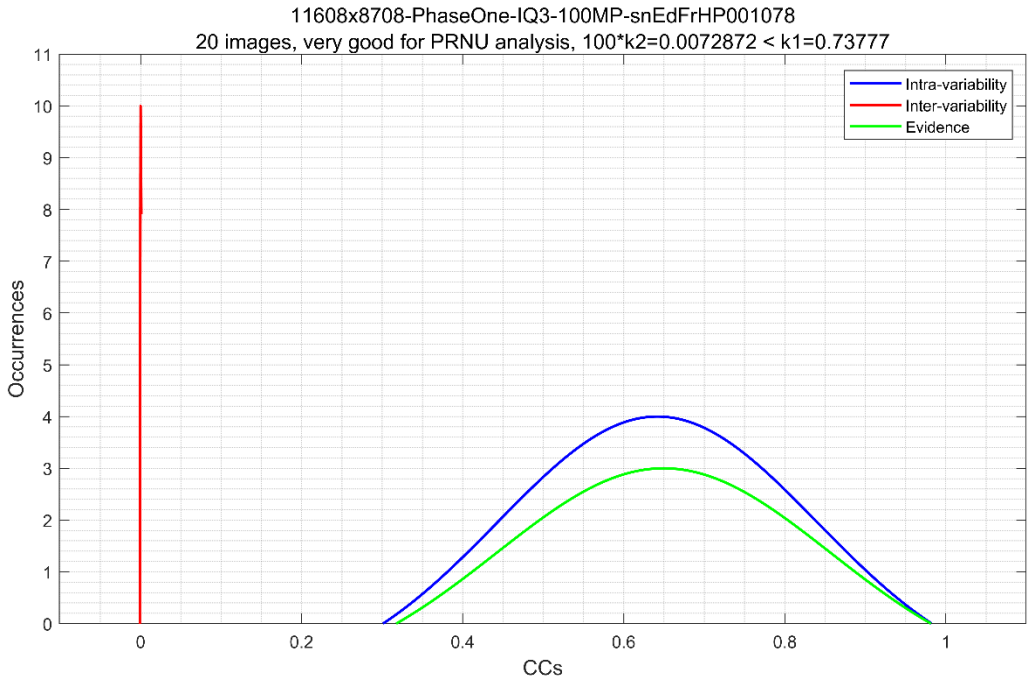


```
Computes CC1, CC2...

ans =

   0.0001    0.7378

  -0.0002    0.7824

20 images, very good for PRNU analysis, 100*k2=0.0072872 < k1=0.73777

-------------------------------------------------------------------------

11608x8708-PhaseOne-IQ3-100MP-snEdFrHP001078
```

Figure 9 Phase One IQ3 100MP PRNU Suitability Test

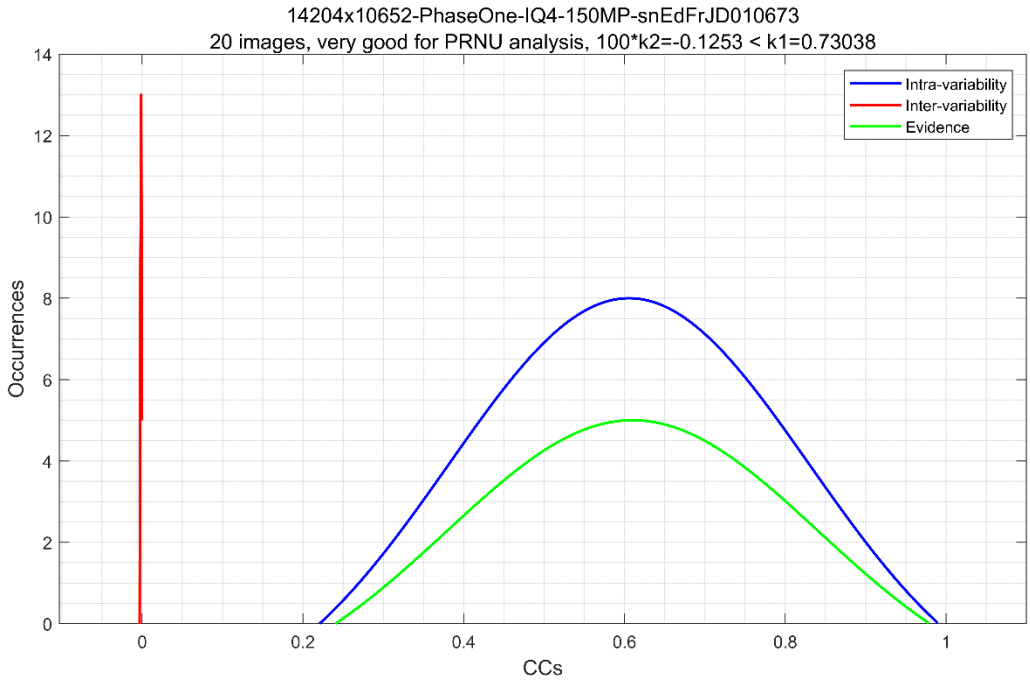


```
Computes CC1, CC2...

ans =

   0.0007    0.7781

   0.0011    0.8505

24 images, very good for PRNU analysis, 100*k2=0.067744 < k1=0.77806

--------------------------------------------------------------------------------

8272x6200-Hassleblad-X1DII-50C-snEdFr565101AB529F
```

Figure 10 Phase One IQ4 150MP PRNU Suitability Test

PRNU Extraction

Once confiremed the flat field images were suitable, the PRNU was extracted and displayed. This was achieved by taking the noise residuals of the reference flat field images and convert them to a grayscale signal. First, the fingerprint is estimated in each of the three color channels (red, blue, green). Then, the channels are combined using the common linear transformation RGB → grayscale, the sample mean is subtracted and averages of each column and each row in each of four sub-sampled 2-D signals

corresponding to four types of pixels in the Bayer CFA are subtracted from all elements. This "Zero-Mean" procedure removes a large portion of Non Unique Artifacts introduced by demosaicking (that is noise that can be found in cameras from the same make and model, making them not unique to the sample camera). To remove any residual artifacts from the estimated fingerprint, the fingerprint was finally filtered using an adaptive Wiener filter in the frequency domain (7).

The following images are the extracted PRNU noise from the reference flat field image set.

Figure 11 FUJIFILM GFX 50s Extracted PRNU Pattern

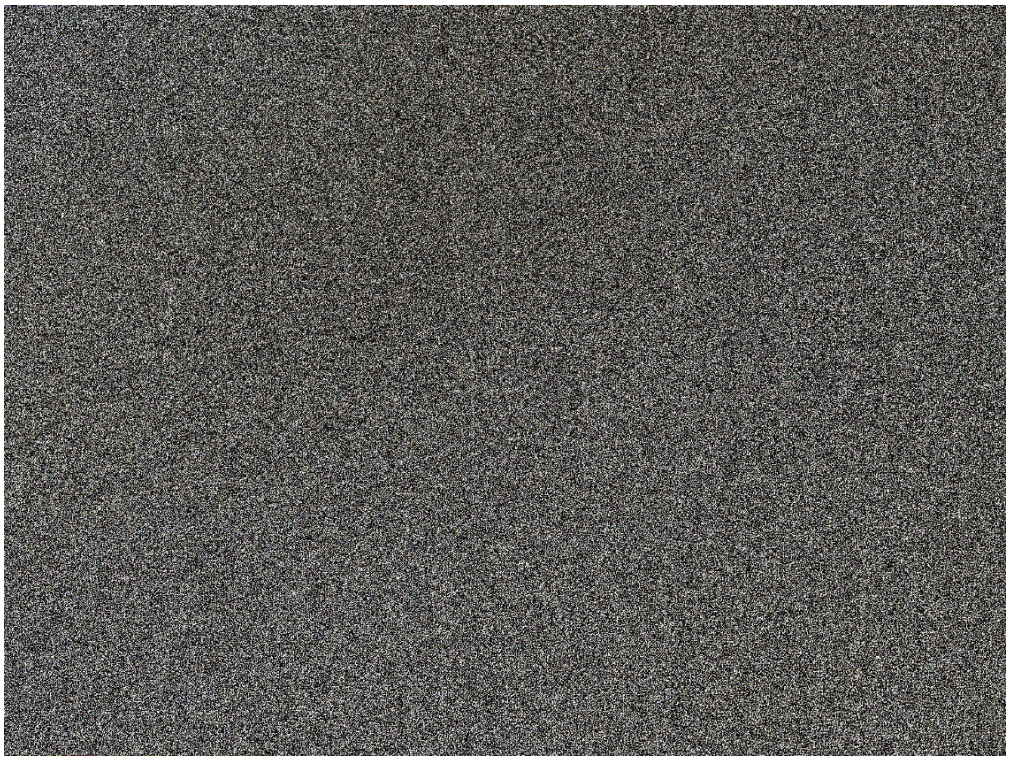

Figure 12 FUJIFILM GFX 100 Extracted PRNU Pattern

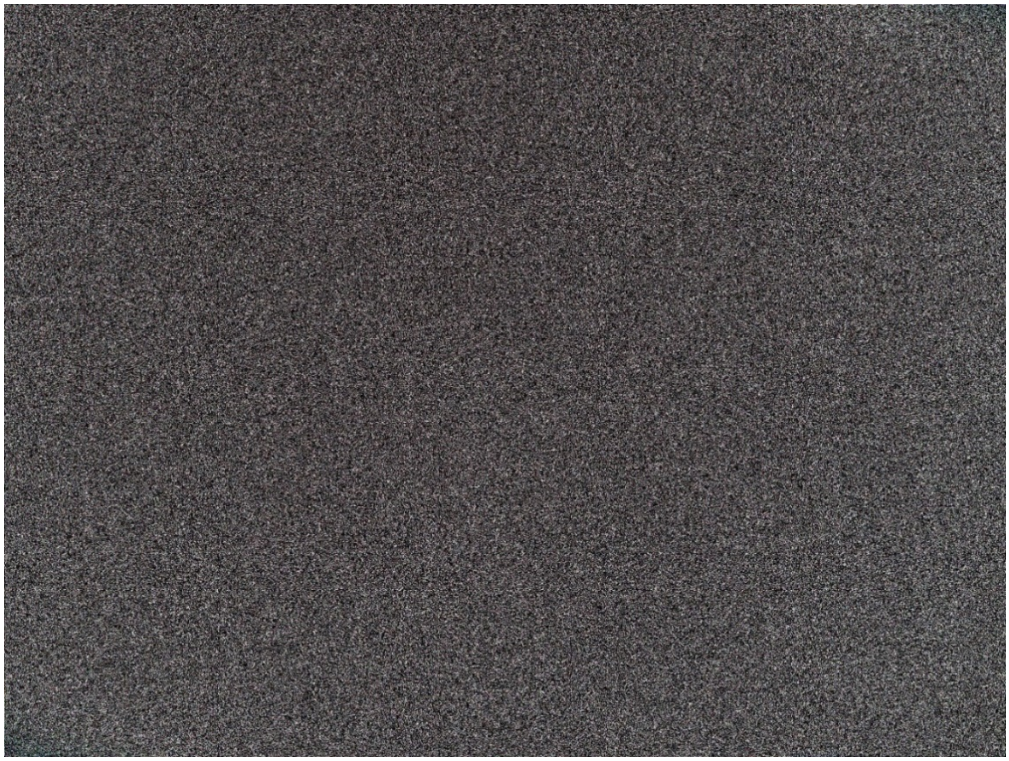

Figure 13 Hasselblad X1DII 50c Extracted PRNU Pattern

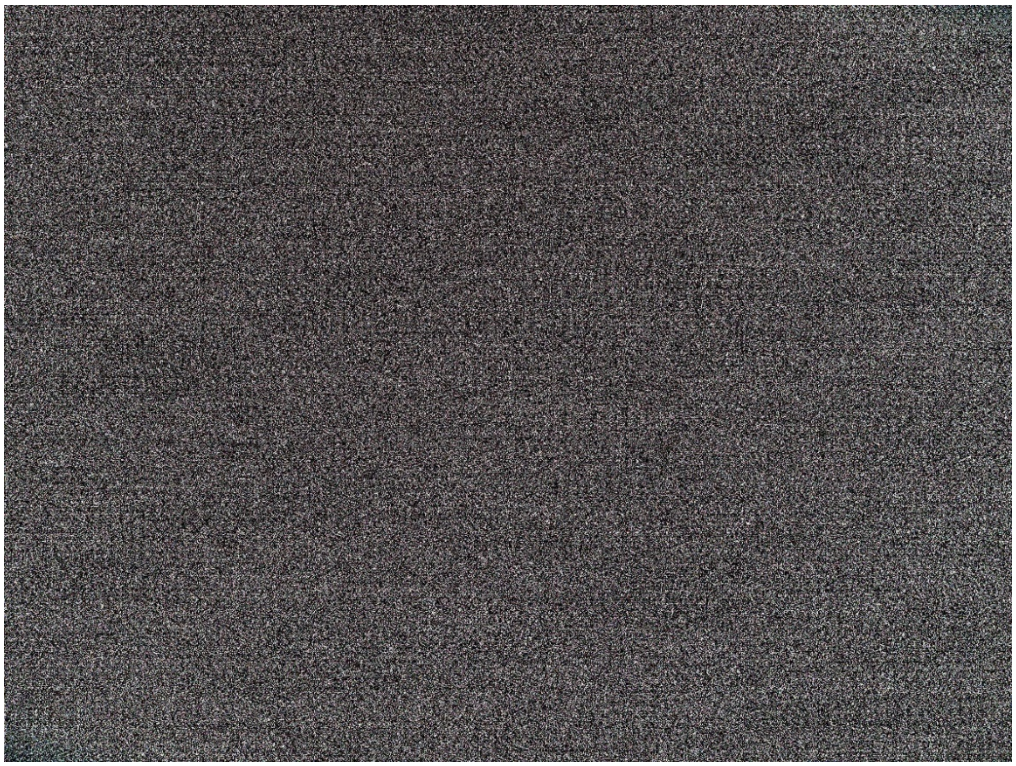

Figure 14 Hasselblad H6D 100c Extracted PRNU Pattern

Figure 15 Phase One IQ3 100MP Extracted PRNU Pattern

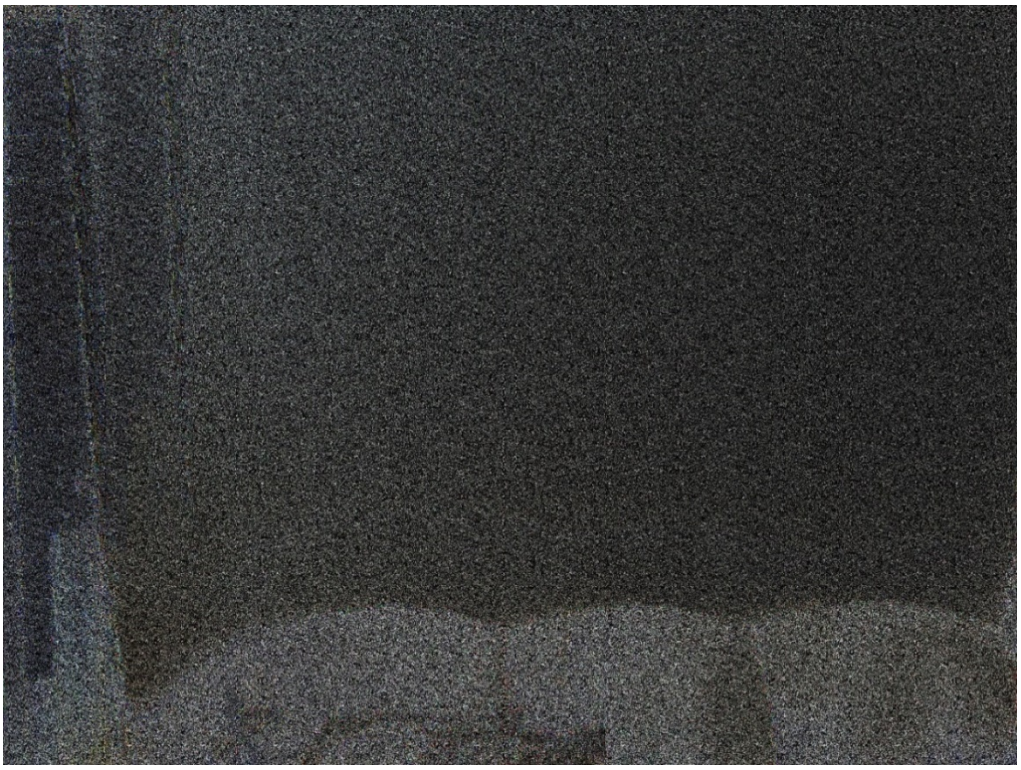

Figure 16 Phase One IQ4 150MP Extracted PRNU Pattern

Note the subtle outline still visible in Figure 16. This was due to the flat field images containing part of some furniture that was overlooked when colleting the flat field images.

CHAPTER III

SOURCE CAMERA COMPARISON

The extracted PRNU was then used to compare a natural scene reference image taken with the reference flat field cameras, and a small open source image database created for this research. PRNU noise was obtained by suppressing scene content from an image with a denoising filter and then averaging the noise residuals. In this study, Gaussian denoising filter, and Wiener denoising filter were used to suppress scene images. The Gaussian filter removes noise by blurring an image. It achieves this by distributing pixels in Gaussian (bell-shaped) distribution across the entire image. The Wiener filter both recovers an image from blurring of a lowpass filter (inverse filtering) and reduces noise by smoothing at the same time, it removes additive noise and inverts the blurring simultaneously (23). Two methods were used to study the accuracy and reliability in comparing between different cameras of the same make and model. Note the appendix will contain figures from all camera comparisons.

In order to conduct this analysis, open source RAW images and some JPEG images were obtained from www.dpreview.com, www.photographyblog.com, www.flickr.com, www.phaseone.com, www.hasselblad.com, and www.FUJIFILM.com, to build a small database of images. All open source RAW images were converted to TIFF files for comparison. The open source images collected were of natural scenes with normal dynamic range and exposure.

Correlation Coefficient (CC) was used to establish the relationship between the source camera and the reference image. Mathematically, CC shows the relationship between two sets of data by evaluating how the values change with relation to each other. CC returns values between -1 and 1, where 1 indicates a strong positive relationship, 0 indicates no correlation, and -1 indicates a strong negative relationship. The intra-variability and inter-variability was calculated. Log Likelihood Ratio (LLR) was used to compare the likelihood the reference image was taken with the sample camera or the open source camera(s). This calculation was then used to determine if the hypothesis the reference

image was taken with the suspect camera either has support, limited support, is inconclusive, or has no support. A larger LLR number represents a greater likelihood the reference images came from that camera. Result tables were color coded green to represent a correct attribution, or correct elimination. Color coded red represents an incorrect identification called false positive, or incorrect elimination called false rejection. Limited support and inconclusive results were color coded gray.

FUJIFILM GFX 50s

A natural scene reference image (_DSF1055.tif) taken with a FUJIFILM GFX 50S camera was compared against flat field images from the source camera (snEdFr71002897), and a set of natural scene images from an open source camera of the same make and model (snDPRdb71001454). The Gaussian method showed limited support for both cameras. It did not correctly attribute the source camera, nor correctly eliminate the open source camera. The Wiener method was inconclusive for the open source camera, and correctly attributed the reference image to the source camera. The Wiener method performed better than the Gaussian method.

Table 3 FUJIFILM GFX 50s Reference Image from snEdFr71002897 Results

Camera used **FUJIFILM GFX 50S**	Gaussian	Wiener
snDPRdb71001454	Limited Support	Inconclusive
snEdFr71002897 source	Limited Support	Has Support

```
----------Evidence----------
Evidence file: _DSF1055.tif
----------Reference----------
2.2268 => 8256x6192-Fuji-GFX-50S-snDPRdb71001454
2.0514 => 8256x6192-Fuji-GFX-50S-snEdFr71002897
```

Figure 17 Gaussian Method FUJIFILM GFX 50s Log Likelihood Ratio Results

```
----------Evidence----------
Evidence file: _DSF1055.tif
----------Reference----------
920.1153 => 8256x6192-Fuji-GFX-50S-snEdFr71002897
1.793 => 8256x6192-Fuji-GFX-50S-snDPRdb71001454
```

Figure 18 Wiener Method FUJIFILM GFX 50s Log Likelihood Ratio Results

FUJIFILM GFX 100

A natural scene reference image (_DSF1093.tif) taken with a FUJIFILM GFX 100 camera was compared against flat field images from the source camera (snEGF76A02867), and seven sets of natural scene images from open source cameras of the same make and model. Six open source cameras were utilized; two cameras with RAW files (sn92001309, sn920001255), three cameras with JPEG files (sn92001020, sn92001023, sn92001142), and one camera with both RAW and JPEG files (sn92A01040). The Gaussian method correctly eliminated the cameras with JPEG files, and showed limited support for two cameras with RAW files. It had a false positive for an open source camera with RAW files (sn920001255), and falsely rejected the source camera. The Wiener method correctly eliminated the cameras with JPEG files, and was inconclusive for two cameras with RAW files. It correctly attributed the reference image to the source camera, but had a false positive for an open source camera with RAW files (sn920001255). Both methods correctly eliminated all JPEG images, yet both methods had a false positive. The Wiener method performed better than the Gaussian method.

Table 4 FUJIFILM GFX 100 Reference Image from snEGF76A02867 Results

Camera used **FUJIFILM GFX 100**	Gaussian	Wiener
sn92A01040 JPEG	No Support	No Support
sn92001020 JPEG	No Support	No Support
sn92001023 JPEG	No Support	No Support
sn92001142 JPEG	No Support	No Support

sn92A01040 RAW	Limited Support	Inconclusive
sn92001309 RAW	Limited Support	Inconclusive
sn920001255 RAW	Has Support	Has Support
snEGF76A02867 source	No Support	Has Support

```
----------Evidence----------
Evidence file: _DSF1093.tif
----------Reference----------
7.923 => 11648x8736-Fuji-GFX-100-snDPRall920001255
2.184 => 11648x8736-Fuji-GFX-100-snDPRall92001309
2.0761 => 11648x8736-Fuji-GFX-100-snDPRall92A01040
0.65465 => 11648x8736-Fuji-GFX-100-snEdFr76A02867
0.0058786 => 11648x8736-FUJIFILM-GFX-100-sn92001023-outdoor-20190524
0.0014498 => 11648x8736-FUJIFILM-GFX-100-sn92001023-outdoor-20190705
0.0013964 => 11648x8736-FUJIFILM-GFX-100-sn92001020-indoor-20190627
0.00040234 => 11648x8736-FUJIFILM-GFX-100-sn92A01040-outdoor-20190531
0.00026888 => 11648x8736-FUJIFILM-GFX-100-sn92A01040-outdoor-20190602
0.00019191 => 11648x8736-FUJIFILM-GFX-100-sn92A01040-outdoor-20190529
4.0999e-05 => 11648x8736-FUJIFILM-GFX-100-sn92001020-outdoor-20190627
```

Figure 19 Gaussian Method FUJIFILM GFX 100 Log Likelihood Ratio Results

```
----------Evidence----------
Evidence file: _DSF1093.tif
----------Reference----------
4.1249 => 11648x8736-Fuji-GFX-100-snEdFr76A02867
3.409 => 11648x8736-Fuji-GFX-100-snDPRall920001255
1.6035 => 11648x8736-Fuji-GFX-100-snDPRall92001309
1.367 => 11648x8736-Fuji-GFX-100-snDPRall92A01040
0.036042 => 11648x8736-FUJIFILM-GFX-100-sn92001023-outdoor-20190705
0.031236 => 11648x8736-FUJIFILM-GFX-100-sn92001020-outdoor-20190627
0.026273 => 11648x8736-FUJIFILM-GFX-100-sn92001023-outdoor-20190524
0.0082169 => 11648x8736-FUJIFILM-GFX-100-sn92A01040-outdoor-20190529
0.0046518 => 11648x8736-FUJIFILM-GFX-100-sn92A01040-outdoor-20190531
0.0033626 => 11648x8736-FUJIFILM-GFX-100-sn92001020-indoor-20190627
0.002312 => 11648x8736-FUJIFILM-GFX-100-sn92A01040-outdoor-20190602
```

Figure 20 Wiener Method FUJIFILM GFX 50s Log Likelihood Ratio Results

Hasselblad X1DII 50c

A natural scene reference image (B7040919.tif) taken with a Hasselblad X1DII 50c camera was compared against flat field images from the source camera (sn565101AB529F), and sets of natural scene images from two open source cameras of the same make and model (sn565101AB5307, sn565101AB530C). The Gaussian method correctly eliminated both open source cameras, and was inconclusive for the source camera. The Wiener method correctly eliminated both open source cameras, and was inconclusive for the source camera. Neither method was able to positively identify the source camera.

Table 5 Hasselblad X1DII 50c Reference Image from snEGF76A02867 Results

Camera used **Hasselblad X1DII 50c**	Gaussian	Wiener
sn565101AB530C	No Support	No Support
sn565101AB5307	No Support	No Support
sn565101AB529F source	Inconclusive	Inconclusive

```
-------------------Evidence-------------------
Evidence file: B7040919.tif
-------------------Reference------------------
1.3958 => 8272x6200-Hassleblad-X1DII-50C-snEdFr565101AB529F
0.3017 => 8272x6200-Hassleblad-X1DII-50C-sn565101AB5307
0.27916 => 8272x6200-Hassleblad-X1DII-50C-sn565101AB530C
```

Figure 21 Gaussian Method Hasselblad X1DII 50c Log Likelihood Ratio Results

```
-------------------Evidence-------------------
Evidence file: B7040919.tif
-------------------Reference------------------
1.3201 => 8272x6200-Hassleblad-X1DII-50C-snEdFr565101AB529F
0.4069 => 8272x6200-Hassleblad-X1DII-50C-sn565101AB530C
0.36728 => 8272x6200-Hassleblad-X1DII-50C-sn565101AB5307
```

Figure 22 Wiener Method Hasselblad X1DII 50c Log Likelihood Ratio Results

Hasselblad H6D 100c

A natural scene reference image (B0000031.tif) taken with a Hasselblad H6D 100c camera was compared against flat field images from the source camera (sn54520225540E), and a set of natural scene images from an open source camera of the same make and model (sn54520225536). The Gaussian method correctly eliminated the open source camera, and correctly attributed the reference image to the source camera. The Wiener method correctly eliminated the open source camera, and correctly attributed the reference image to the source camera. Both methods correctly attributed the source camera and eliminated the open source camera.

Table 6 Hasselblad H6D 100c Reference Image from sn54520225540E Results

Camera used **Hasselblad H6D 100c**	Gaussian	Wiener
sn54520225536	No Support	No Support
sn54520225540E source	Has Support	Has Support

```
----------Evidence----------
Evidence file: B0000031.tif
----------Reference----------
6.0045 => 11600x8700-Hassleblad-H6D-100C-snEdFr54520225540E
0.048243 => 11600x8700-Hasselblad-H6D-100c-snEdFr54520225536
```

Figure 23 Gaussian Method Hasselblad H6D 100c Log Likelihood Ratio Results

```
----------Evidence----------
Evidence file: B0000031.tif
----------Reference----------
3.3766 => 11600x8700-Hassleblad-H6D-100C-snEdFr54520225540E
0.026363 => 11600x8700-Hasselblad-H6D-100c-snEdFr54520225536
```

Figure 24 Wiener Method Hasselblad H6D 100c Log Likelihood Ratio Results

Phase One IQ3 100MP

A natural scene reference image (CF008259.tif) taken with a Phase One IQ3 100MP camera was compared against flat field images from the source camera (snHP001078), a set of natural scene images from an open source camera (snIG011142), and both flat field and natural scene sets of images from a camera of the same make and model (snHP001634). The Gaussian method correctly eliminated one of the open source cameras. It correctly eliminated the flat field set of images from the second open source camera, but had limited support for the natural scene set of images from that camera (snHP001634). It correctly attributed the reference image to the source camera. The Wiener method correctly eliminated one of the open source cameras. It correctly eliminated the flat field set of images from the second open source camera, but had a false positive for the natural scene set of images from that camera (snHP001634). It correctly attributed the reference image to the source camera. Both methods correctly identified the source camera, but the Wiener method had a false positive.

Table 7 Phase One IQ3 100MP Reference Image from snHP001078 Results

Camera used **Phase One IQ3 100MP**	Gaussian	Wiener
snIG011142	No Support	No Support
snHP001634 (flat field)	No Support	No Support
snHP001634 (natural scene)	Limited Support	Has Support
snHP001078 source	Has Support	Has Support

```
------------------Evidence------------------
Evidence file: CF008259.tif
------------------Reference-----------------
10.4939 => 11608x8708-PhaseOne-IQ3-100MP-snEdFrHP001078
2.2616 => 11608x8709-PhaseOne-IQ3-100MP-snTEWHP001634out
0.51505 => 11608x8708-PhaseOne-IQ3-100MP-snTEWHP001634
0.0014213 => 11608x8709-PhaseOne-IQ3-100MP-snIRIG011142
```

Figure 25 Gaussian Method Phase One IQ3 100MP Log Likelihood Ratio Results

```
----------Evidence----------
Evidence file: CF008259.tif
----------Reference----------
14.0131 => 11608x8709-PhaseOne-IQ3-100MP-snTEWHP001634out
3.0122 => 11608x8708-PhaseOne-IQ3-100MP-snEdFrHP001078
0.3793 => 11608x8708-PhaseOne-IQ3-100MP-snTEWHP001634
0.0028195 => 11608x8709-PhaseOne-IQ3-100MP-snIRIG011142
```

Figure 26 Wiener Method Phase One IQ3 100MP Log Likelihood Ratio Results

Phase One IQ4 150MP

A natural scene reference image (Capture11829.tif) taken with a Phase One IQ4 150MP camera was compared against flat field images from the source camera (snEdFrJD010673), and a set of natural scene images from an open source camera of the same make and model (snJD020741). Note this 151 megapixels sensor was the largest one studied, which caused some computing memory issues in the processing. The original TIFF conversion files were 14204x10652 pixels and around 840 megapixels file size each. This caused a memory error when conducting the camera comparison tests. Neither TIFF lossless compression nor JPEG compression were able to solve the memory issues. The error may arise from an array size limitation on the version of Matlab used in this study. As a solution, images from this camera were down-sampled to 1601x8700 pixels, which allowed the algorithm to process the images without any further errors. The Gaussian method had a false positive for the open source camera. It correctly attributed the reference image to the source camera. The Wiener method was inconclusive for the open source camera. It correctly attributed the reference image to the source camera. Both methods correctly identified the source camera, but the Gaussian method had a false positive.

Table 8 Phase One IQ4 150MP Reference Image from snJD010673 Results

Camera used **Phase One IQ4 150MP**	Gaussian	Wiener
snJD020741	Has Support	Inconclusive
snJD010673 source	Has Support	Has Support

```
------------------Evidence------------------
Evidence file: Capture11829.tif
------------------Reference-----------------
4.5279 => 11601x8700 down sampled from 14204x10652-PhaseOne-IQ4-150-snDPRallJD020741
3.1936 => 11601x8700 down sampled from 14204x10652-PhaseOne-IQ4-150MP-snEdFrJD010673
```

Figure 27 Gaussian Method Phase One IQ4 150MP Log Likelihood Ratio Results

```
------------------Evidence------------------
Evidence file: Capture11829.tif
------------------Reference-----------------
4.0585 => 11601x8700 down sampled from 14204x10652-PhaseOne-IQ4-150MP-snEdFrJD010673
1.3039 => 11601x8700 down sampled from 14204x10652-PhaseOne-IQ4-150-snDPRallJD020741
```

Figure 28 Wiener Method Phase One IQ4 150MP Log Likelihood Ratio Results

CHAPTER IV

CONCLUSION

This was a preliminary study of medium format sensors and the background Photo Response Non-Uniformity with flat field images. Some expected and some unexpected results arose during the analysis of these sensors. The denoising filters used were the Gaussian and Wiener methods. Overall, the Wiener method performed better than the Gaussian method for camera comparison, but not as well as in other studies. The Gaussian method correctly attributed or eliminated cameras 12 times with 3 false positive over 21 tests (57.2% success rate, 14.3% error rate). The Wiener method correctly attributed or eliminated cameras 14 times with 1 false positive over 21 tests (66.7% success rate, 4.78% error rate). Both methods correctly excluded all JPEG images included in the tests. The Wiener method was more reliable than the Gaussian method, but clearly both methods have some limitations when dealing with medium format sensors, either from the file size or the higher quality of these sensors. Other methods have been developed that may handle camera comparison better. Future research should include possibly a Wavelet methods (3), a Block Matching and 3D (BM3D) filter method (24), and/or an Anisotropic Diffusion (AD) filtering schemes (25). Camera comparison was done with cross correlation, but other methods like Peak to Correlation Energy (PCE) or Maximum Likelihood Estimate (MLE) exist that may prove to be more reliable in future research.

One of the experimental goals of this thesis was working with RAW image data to analyze the full capabilities of these superior sensors. Matlab does not ingest RAW files directly, so they had to be converted into uncompressed TIFF files. An issue with TIFF files is they tend to grow in size when converting from RAW files, growing from 50 MB – 150 MB to 146 MB – 868 MB. This not only makes collecting large sets of images difficult in file management but also working with these files is extremely time consuming. Another limitation in TIFF conversion was the degradation in bit depth from the 14 or

16 bits per channel to only 8 bits. This defeats one of the advantages of medium format cameras over previously researched consumer level cameras.

Creating a proper database is essential for source camera comparison. This proved to be a challenge for this type of cameras. Medium format cameras are not consumer level, they tend to range in cost from $5,000 USD to $52,000 USD. The high sticker price means they are mostly sold in specialty camera stores, and places that do have them will tend to only have one model on display, making it difficult to collect multiple source samples. Sample images can be found on open source sites, but RAW files are not typically available. Open source samples are often limited in quantity of images and in the variety of same make and model cameras. Also, no flat field images were found on open source sites for these cameras. For proper comparison, it would be ideal to have a database of multiple cameras of flat field images, with 50 or more images from each camera. One last limitation in creating a comparative database is all the medium format cameras used in this research had their own unique sensor resolution. That is, none of the sensors analyzed had the same number of pixels as any other. This undoubtably introduced some intra-make/model fixed pattern noise which made camera comparison less reliable.

In conclusion, medium format cameras produce unrivaled images in quality, definition, clarity, dynamic range, and color tones. The higher build quality of these massive sensors produces less background noise than consumer cameras. One might think a larger file would have more background noise for camera comparison, but that isn't the case. From a forensic perspective, the higher quality of medium format sensors makes correct attribution and elimination of a source camera more difficult than a cheaper consumer level camera.

REFERENCES

1. Rista J. What causes banding noise in CMOS sensors? 2019 [Available from: https://photo.stackexchange.com.

2. Martinec E. Noise, Dynamic Range and Bit Depth in Digital SLRs 2008 [Available from: http://theory.uchicago.edu/~ejm/pix/20d/tests/noise/.

3. Fridrich J. Digital Image Forensics Using Sensor Noise

4. United States of America v Nathan Allen Railey. United States District Court: Southern District of Alabama; 2011.

5. Said A, Lukas J, Apostolopoulos JG, Fridrich J, Goljan M. Determining digital image origin using sensor imperfections. Image and Video Communications and Processing 20052005.

6. Sargent JTG, A. Test Report Approval, nonpublished communication to the FBI. Law Enforcement Analysis Facility. 2009.

7. Goljan MF, J.; Filler, T. Large Scale Test of Sensor Fingerprint Camera Identification. Proc SPIE, Media Forensics and Security. 2009;7254.

8. Rosenfeld KS, Husrev Taha. A Study of the Robustness of PRNU-based Camera Identification. Proc SPIE, Media Forensics and Security. 2009;72540M.

9. M. Chen JF. Determining image origin and integrity using sensor noise. IEEE Transactions on Information Forensics and Security. 2008;3:74-90.

10. Li C. Source camera identification using enhanced sensor pattern noise. IEEE Trans Image Process. 2010;5:280-7.

11. Li C, Li, Y. Color-decoupled photo response non-uniformity for digital image forensics. IEEE Trans Circuits System Video Technology. 2012;22(260-271).

12. Cortiana A, Conotter, Valentina, Boato, G., Natale, F.G.B. Performance comparison of

denoising filters for source camera identification. SPIE Electronic Imaging. 2011.

13. Hu Y, Jian, C., Li, C. Source camera identification using large components of sensor pattern noise. Proceedings of Int Conf Computer Science Applications. 2009;23:1-5.

14. Kang X, Jiansheng, C., Kerui, I. A context-adaptive spn predictor for trustworthy source camera identification. EURASIP Journal on Image and Video Processing. 2014;1.

15. Lin X, Li, C.T. Preprocessing reference sensor pattern noise via spectrum equalization. IEEE Transactions on Information Forensics and Security. 2016;11:126-40.

16. Luka J, Fridrich J, Goljan M. Digital Camera Identification From Sensor Pattern Noise. IEEE Transactions on Information Forensics and Security. 2006;1(2):205-14.

17. Mehrish A, Subramanyam AV, Emmanuel S. Robust PRNU estimation from probabilistic raw measurements. Signal Processing: Image Communication. 2018;66:30-41.

18. Thing YCaVLL. A study on the photo response non-uniformity noise pattern based image forensics in real-world applications. Institute for Infocomm Research. 2012.

19. Fujifilm-x 2019 [Available from: https://fujifilm-x.com/en-us/products/cameras/.

20. Hasselblad Medium Format 2019 [Available from: https://www.hasselblad.com/medium-format/.

21. PhaseOne 2019 [Available from: https://www.phaseone.com/en/Photography/Camera-Technology/Full-Frame-Medium-Format.

22. M. K. Mihcak IK, K. Ramchandran, and P. Moulin. Low-complexity image denoising based on statistical modeling of wavelet coefficients. IEEE Signal Process Lett. 1999(6(12)):300-3.

23. Benjamin Anderson-Sackaney AA-D. Evaluation of Sensor Pattern Noise Estimators for Source Camera Identification. International Journal of Computer and Information Engineering. 2016;10(12).

24. K. Dabov AF, V. Katkovnik, and K. Egiazarian. Image denoising by sparse 3-D transform-domain collaborative filtering. IEEE Transactions on Image Processing. 2007;16(8):2080-95.

25. W.V. Houten ZG. Using Anisotropic Diffusion for Efficient Extraction of Sensor Noise in Camera Identification. Journal of Forensic Sciences. 2012;57:521-7.

APPENDIX

Graphs from camera comparison tests.

FUJIFILM GFX 50s

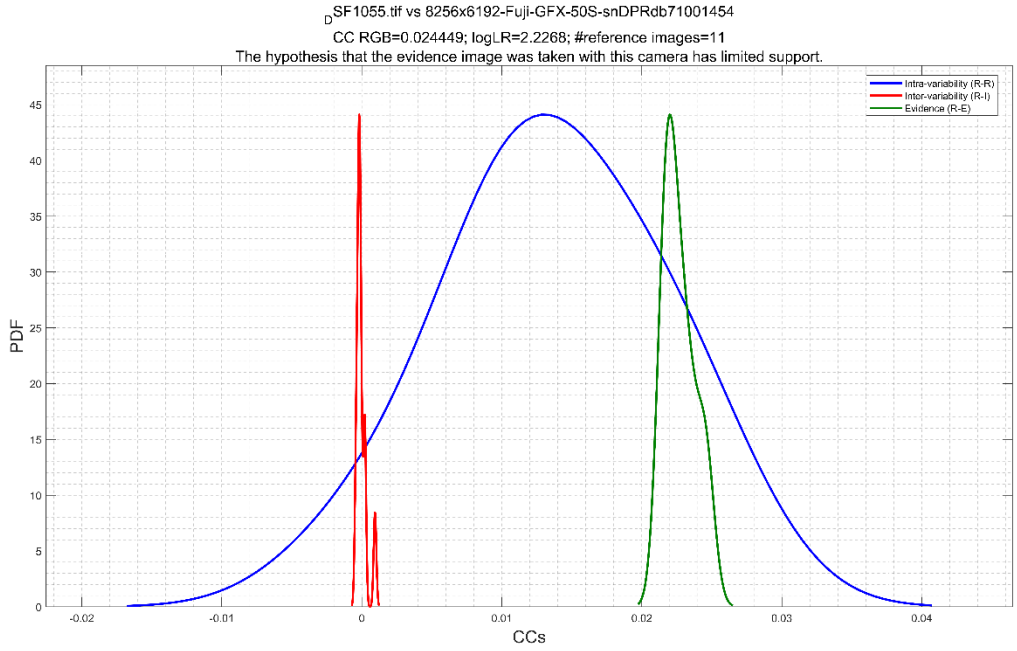

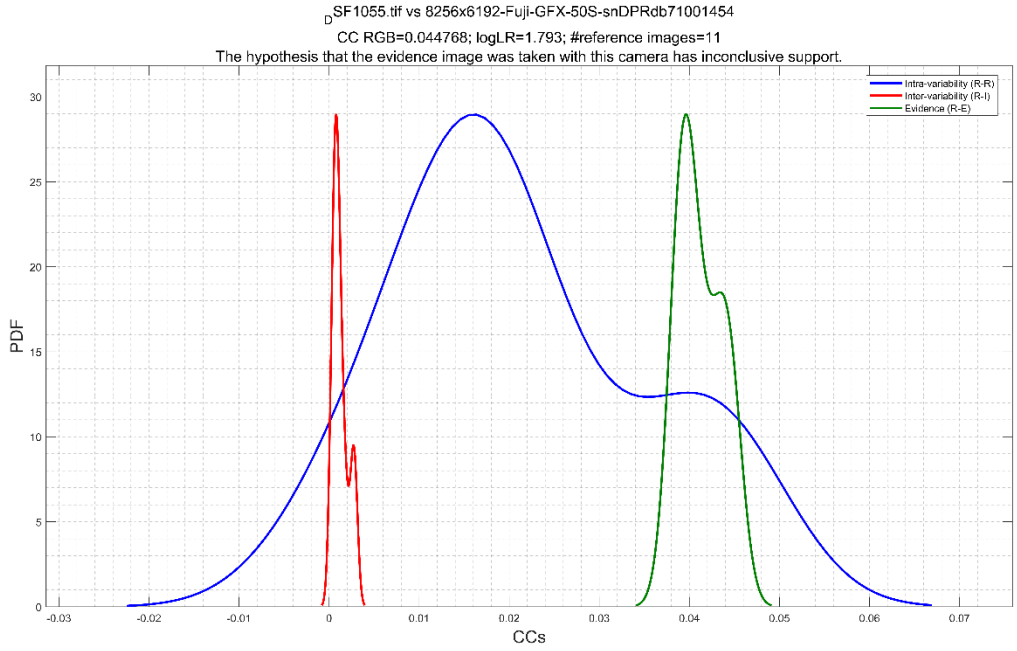

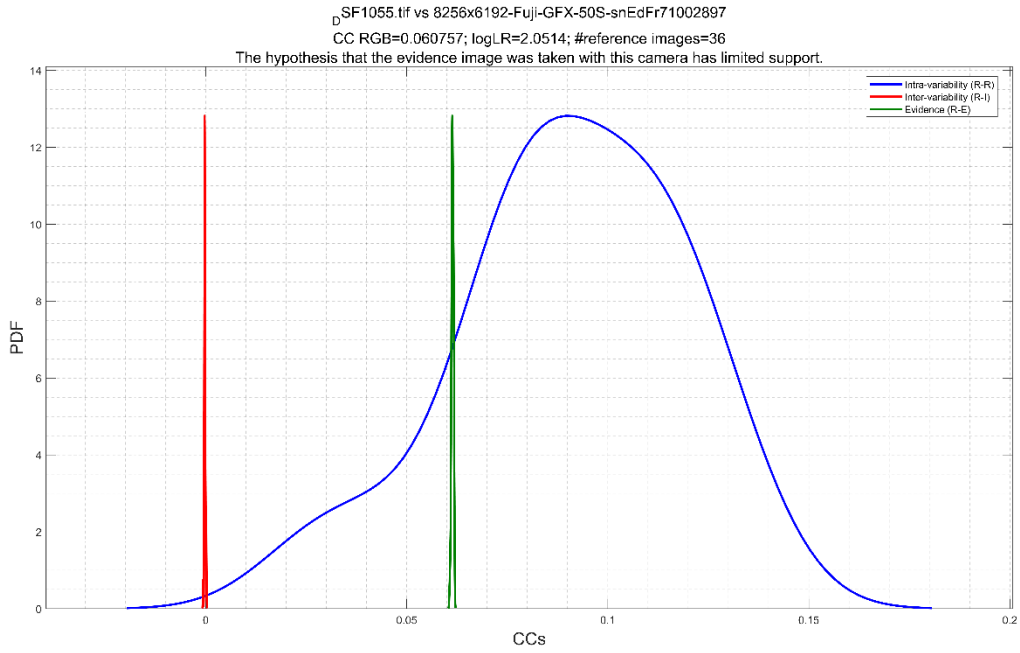
DSF1055.tif vs 8256x6192-Fuji-GFX-50S-snEdFr71002897
CC RGB=0.060757; logLR=2.0514; #reference images=36
The hypothesis that the evidence image was taken with this camera has limited support.
Intra-variability (R-R)
Inter-variability (R-I)
Evidence (R-E)
PDF
CCs

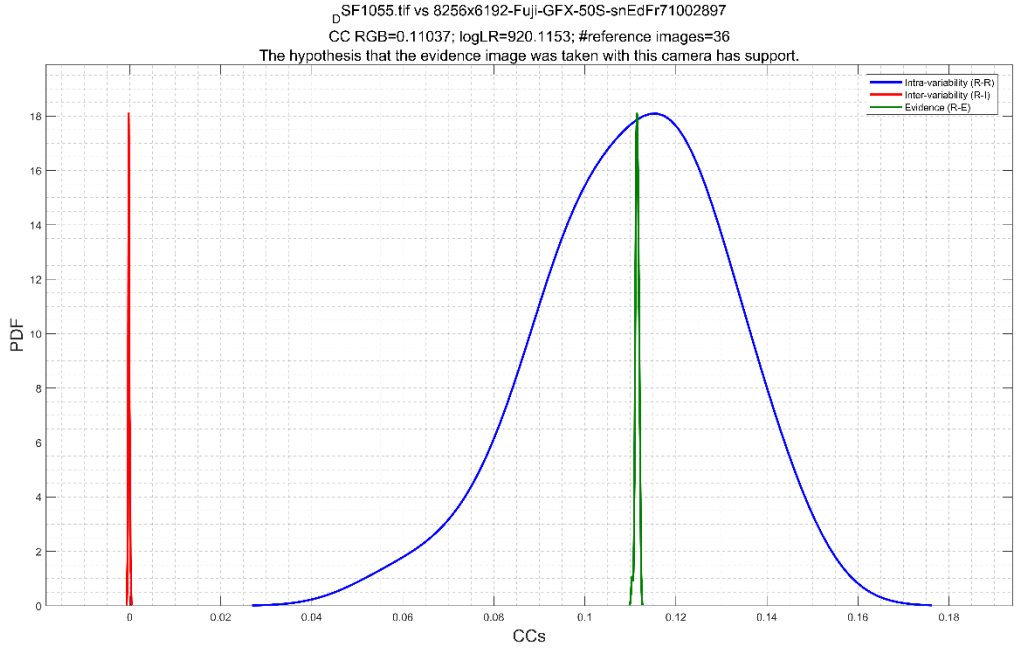
DSF1055.tif vs 8256x6192-Fuji-GFX-50S-snEdFr71002897
CC RGB=0.11037; logLR=920.1153; #reference images=36
The hypothesis that the evidence image was taken with this camera has support.
Intra-variability (R-R)
Inter-variability (R-I)
Evidence (R-E)
PDF
CCs

FUJIFILM GFX 100

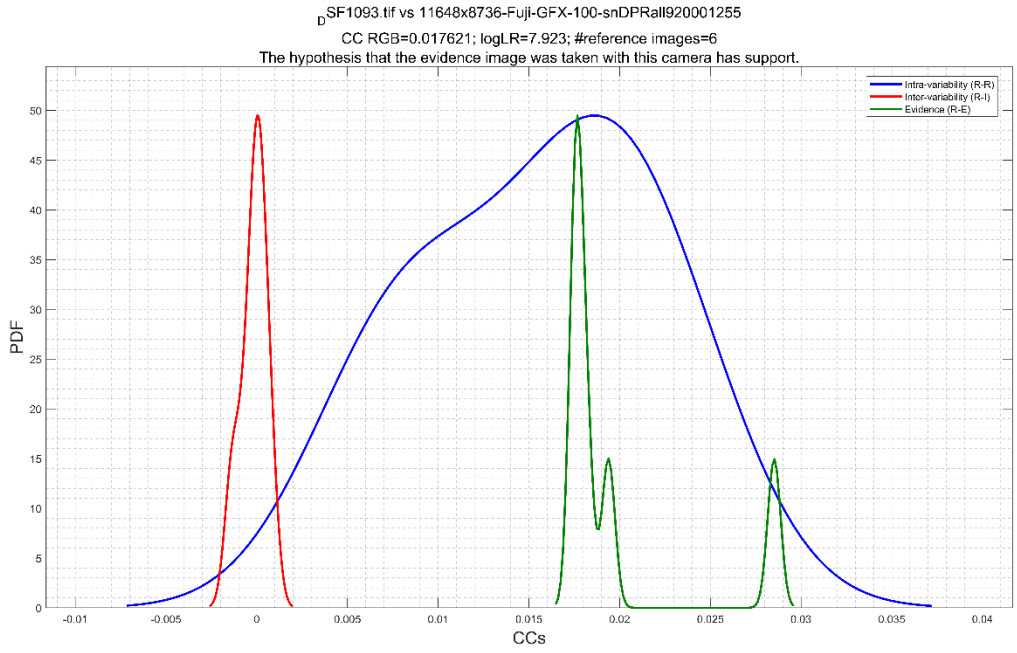

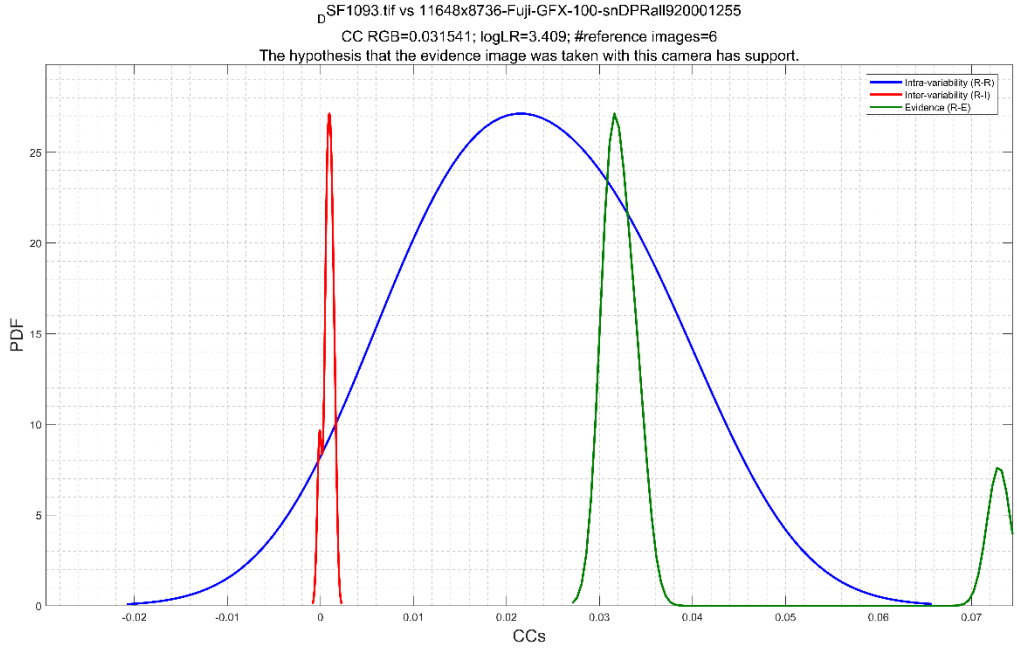

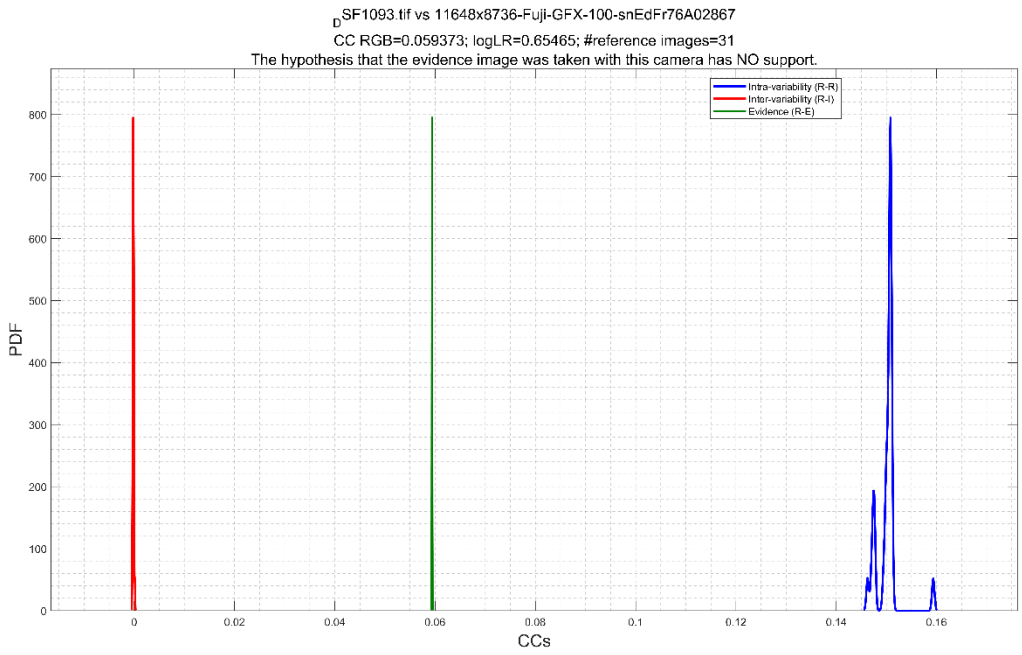
D SF1093.tif vs 11648x8736-Fuji-GFX-100-snEdFr76A02867
CC RGB=0.059373; logLR=0.65465; #reference images=31
The hypothesis that the evidence image was taken with this camera has NO support.
Intra-variability (R-R)
Inter-variability (R-I)
Evidence (R-E)
PDF
CCs

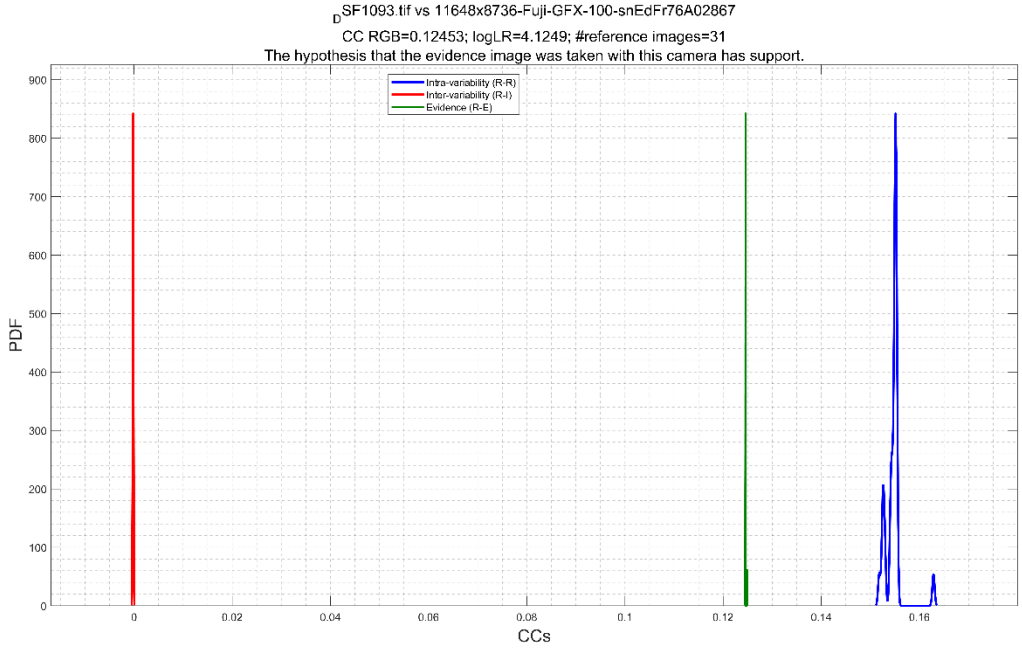
D SF1093.tif vs 11648x8736-Fuji-GFX-100-snEdFr76A02867
CC RGB=0.12453; logLR=4.1249; #reference images=31
The hypothesis that the evidence image was taken with this camera has support.
Intra-variability (R-R)
Inter-variability (R-I)
Evidence (R-E)
PDF
CCs

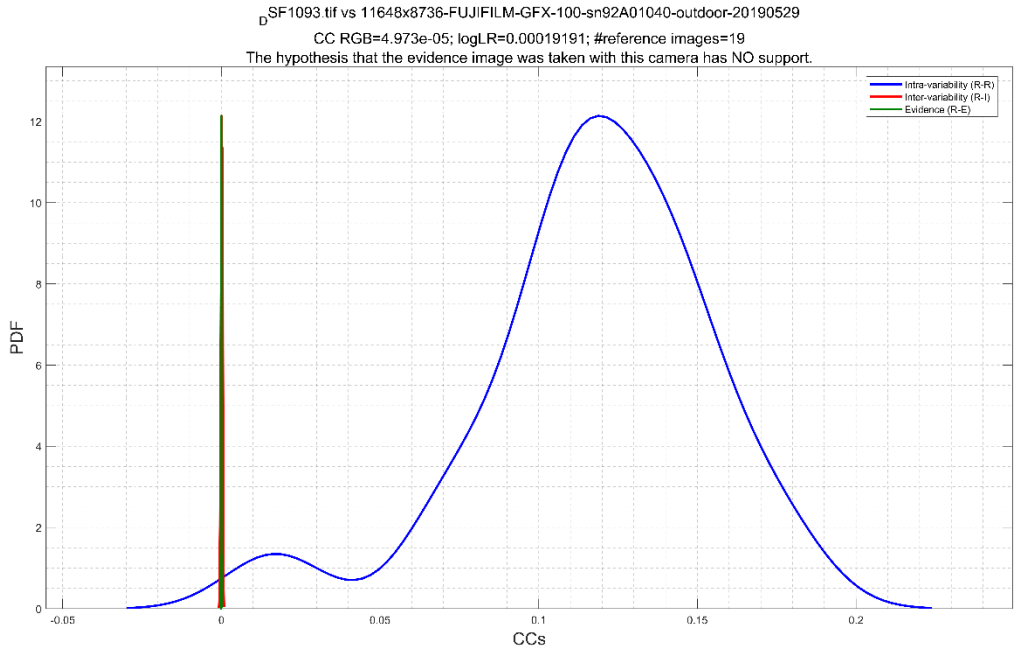
D SF1093.tif vs 11648x8736-FUJIFILM-GFX-100-sn92A01040-outdoor-20190529
CC RGB=4.973e-05; logLR=0.00019191; #reference images=19
The hypothesis that the evidence image was taken with this camera has NO support.
Intra-variability (R-R)
Inter-variability (R-I)
Evidence (R-E)
PDF
CCs

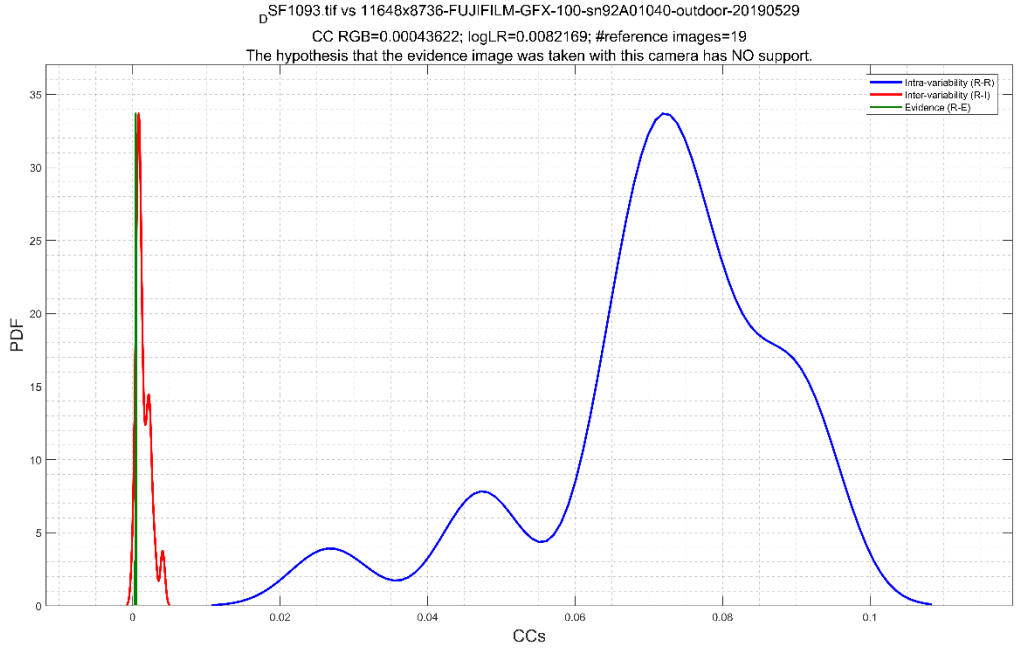
D SF1093.tif vs 11648x8736-FUJIFILM-GFX-100-sn92A01040-outdoor-20190529
CC RGB=0.00043622; logLR=0.0082169; #reference images=19
The hypothesis that the evidence image was taken with this camera has NO support.
Intra-variability (R-R)
Inter-variability (R-I)
Evidence (R-E)
PDF
CCs

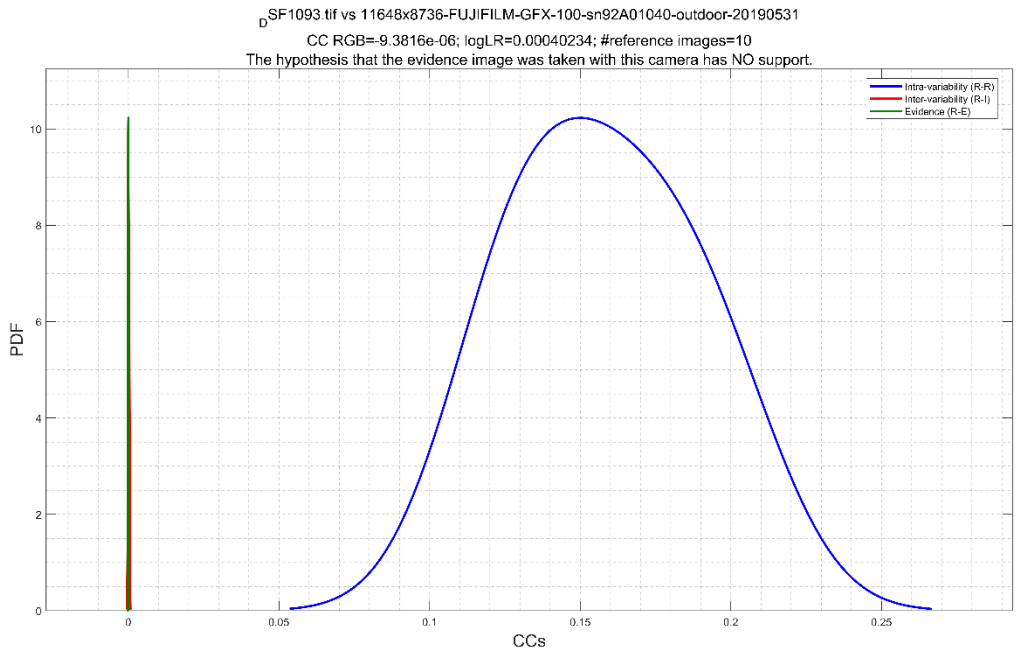
D SF1093.tif vs 11648x8736-FUJIFILM-GFX-100-sn92A01040-outdoor-20190531
CC RGB=-9.3816e-06; logLR=0.00040234; #reference images=10
The hypothesis that the evidence image was taken with this camera has NO support.
Intra-variability (R-R)
Inter-variability (R-I)
Evidence (R-E)
PDF
CCs

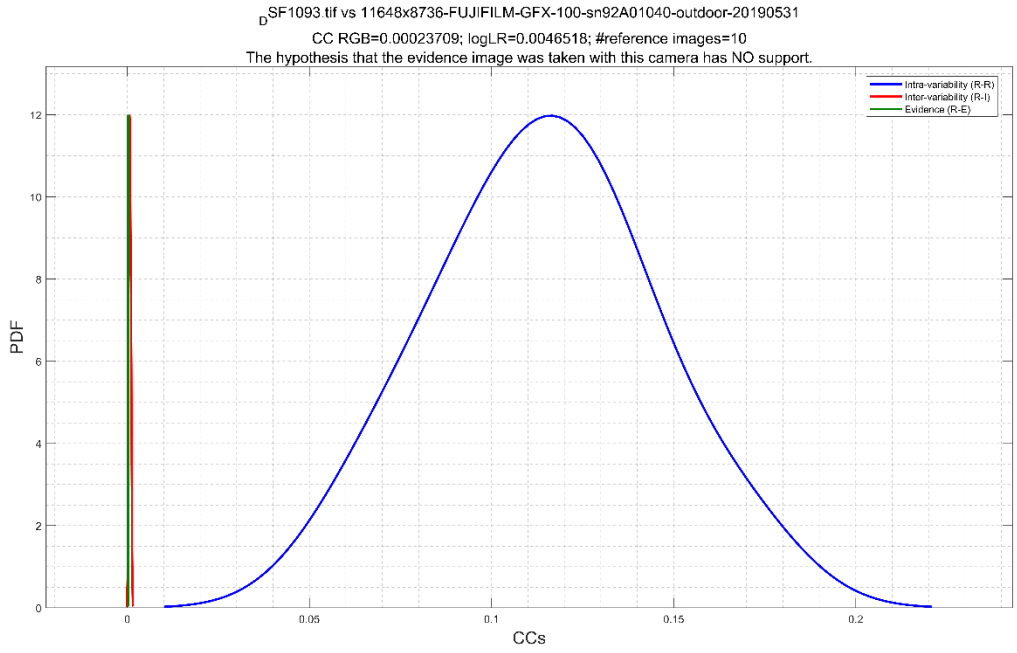
D SF1093.tif vs 11648x8736-FUJIFILM-GFX-100-sn92A01040-outdoor-20190531
CC RGB=0.00023709; logLR=0.0046518; #reference images=10
The hypothesis that the evidence image was taken with this camera has NO support.
Intra-variability (R-R)
Inter-variability (R-I)
Evidence (R-E)
PDF
CCs

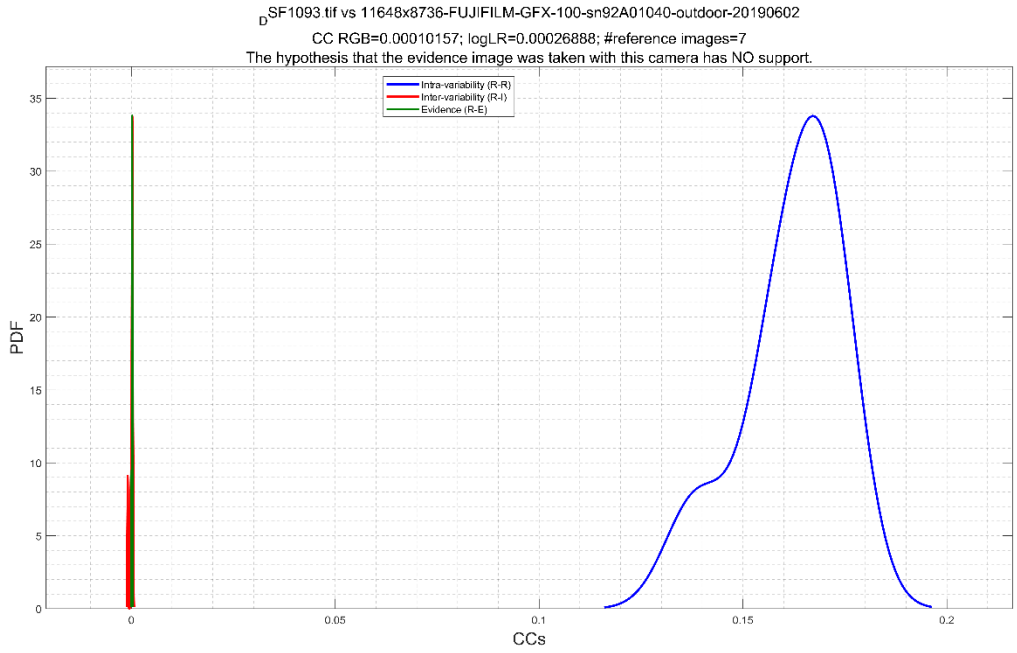
D SF1093.tif vs 11648x8736-FUJIFILM-GFX-100-sn92A01040-outdoor-20190602
CC RGB=0.00010157; logLR=0.00026888; #reference images=7
The hypothesis that the evidence image was taken with this camera has NO support.
Intra-variability (R-R)
Inter-variability (R-I)
Evidence (R-E)
PDF
CCs

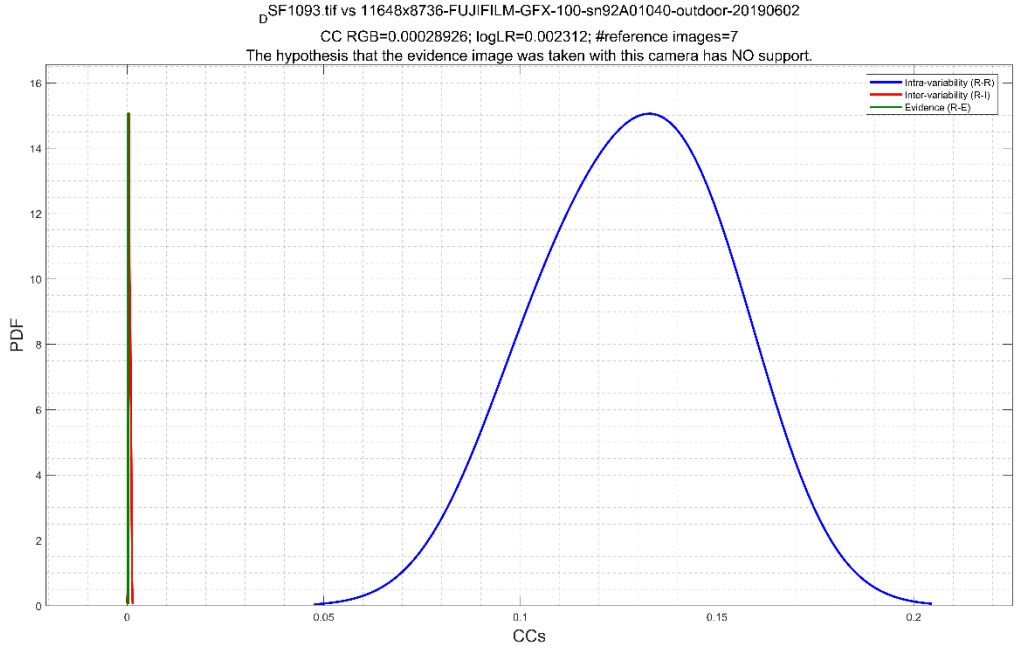
D SF1093.tif vs 11648x8736-FUJIFILM-GFX-100-sn92A01040-outdoor-20190602
CC RGB=0.00028926; logLR=0.002312; #reference images=7
The hypothesis that the evidence image was taken with this camera has NO support.
Intra-variability (R-R)
Inter-variability (R-I)
Evidence (R-E)
PDF
CCs

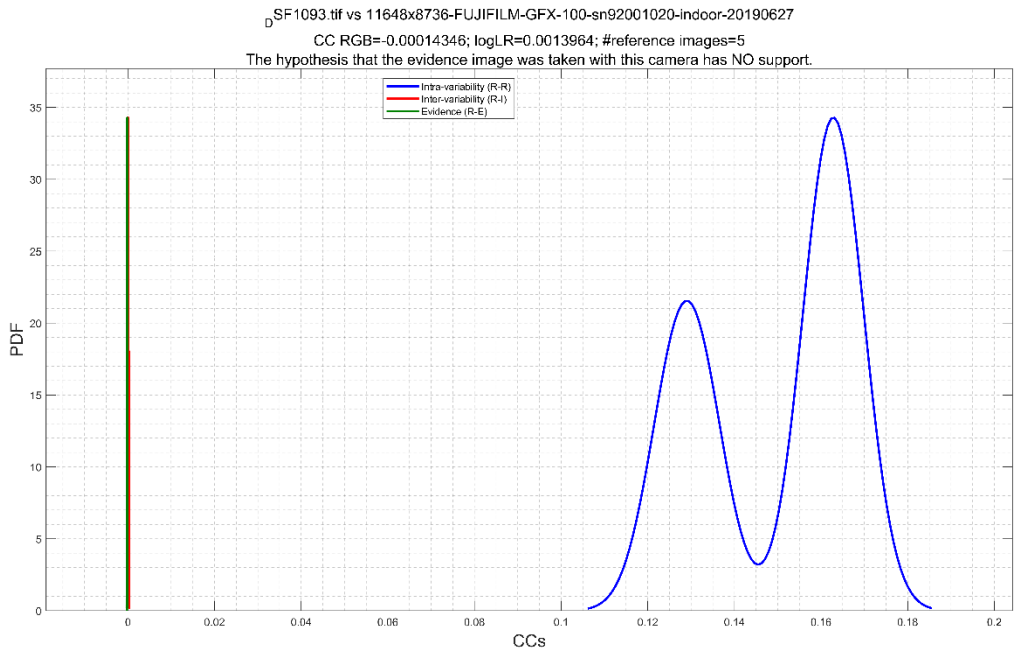
DSF1093.tif vs 11648x8736-FUJIFILM-GFX-100-sn92001020-indoor-20190627
CC RGB=-0.00014346; logLR=0.0013964; #reference images=5
The hypothesis that the evidence image was taken with this camera has NO support.
Intra-variability (R-R)
Inter-variability (R-I)
Evidence (R-E)
PDF
CCs

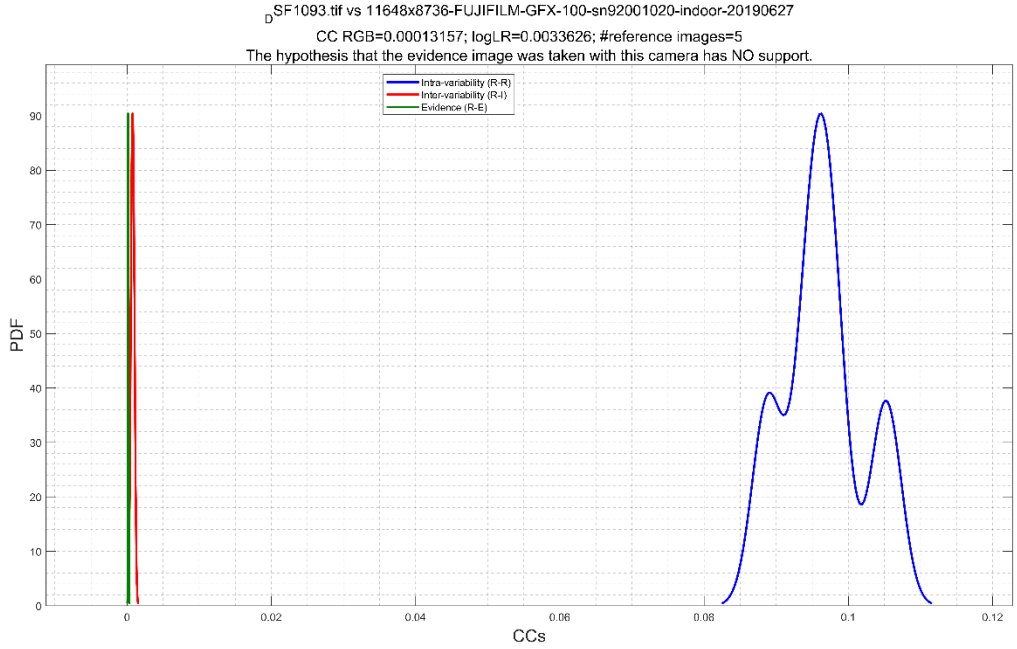
DSF1093.tif vs 11648x8736-FUJIFILM-GFX-100-sn92001020-indoor-20190627
CC RGB=0.00013157; logLR=0.0033626; #reference images=5
The hypothesis that the evidence image was taken with this camera has NO support.
Intra-variability (R-R)
Inter-variability (R-I)
Evidence (R-E)
PDF
CCs

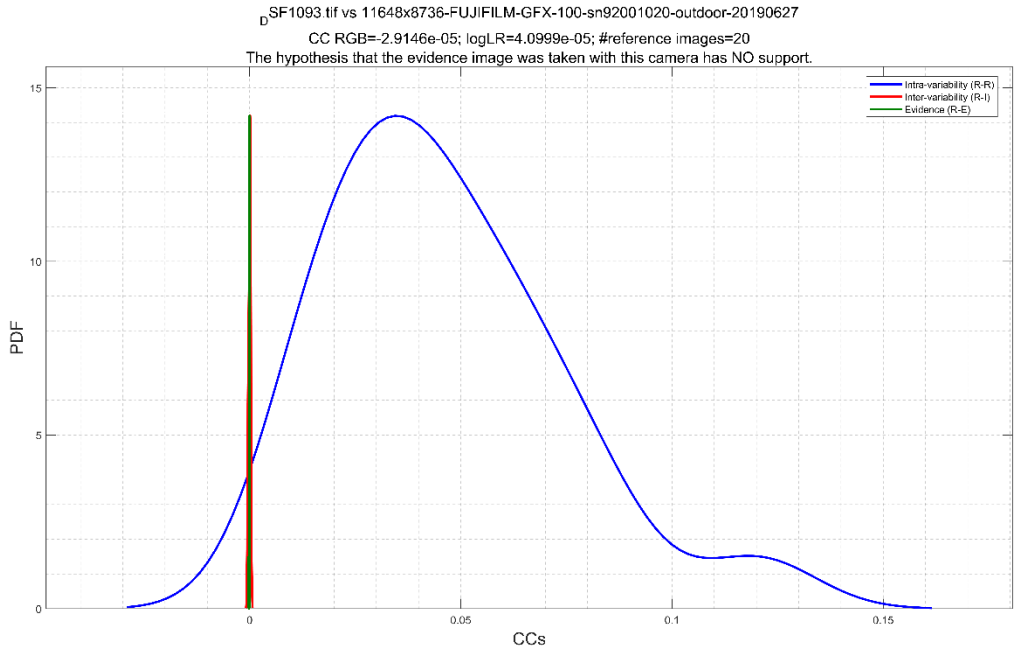
D SF1093.tif vs 11648x8736-FUJIFILM-GFX-100-sn92001020-outdoor-20190627
CC RGB=-2.9146e-05; logLR=4.0999e-05; #reference images=20
The hypothesis that the evidence image was taken with this camera has NO support.
Intra-variability (R-R)
Inter-variability (R-I)
Evidence (R-E)
PDF
CCs
0
5
10
15
0
0.05
0.1
0.15

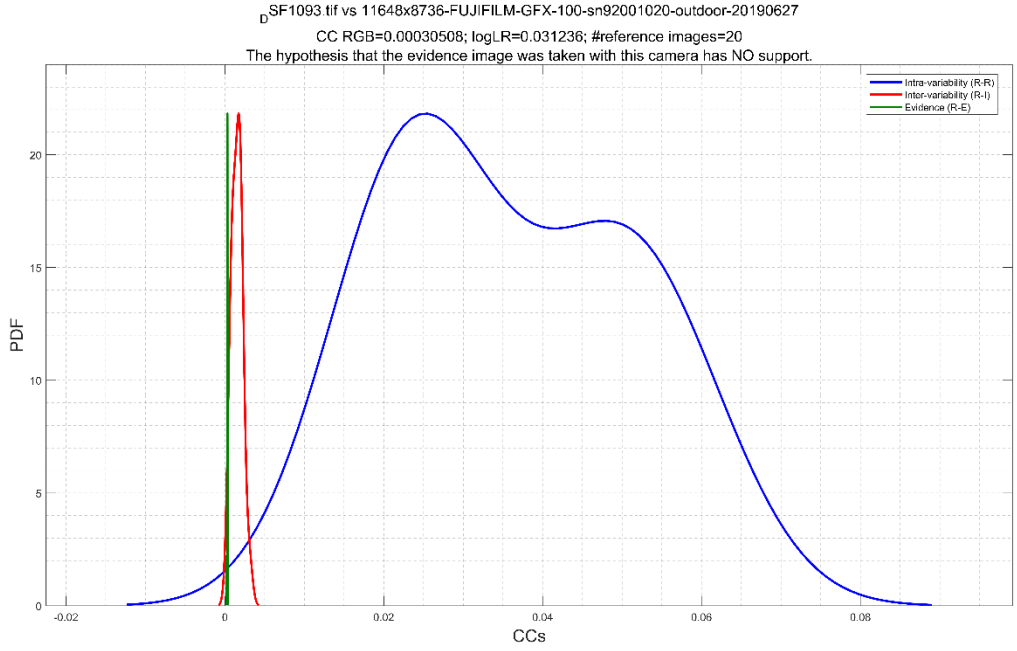
D SF1093.tif vs 11648x8736-FUJIFILM-GFX-100-sn92001020-outdoor-20190627
CC RGB=0.00030508; logLR=0.031236; #reference images=20
The hypothesis that the evidence image was taken with this camera has NO support.
Intra-variability (R-R)
Inter-variability (R-I)
Evidence (R-E)
PDF
CCs
0
5
10
15
20
-0.02
0
0.02
0.04
0.06
0.08

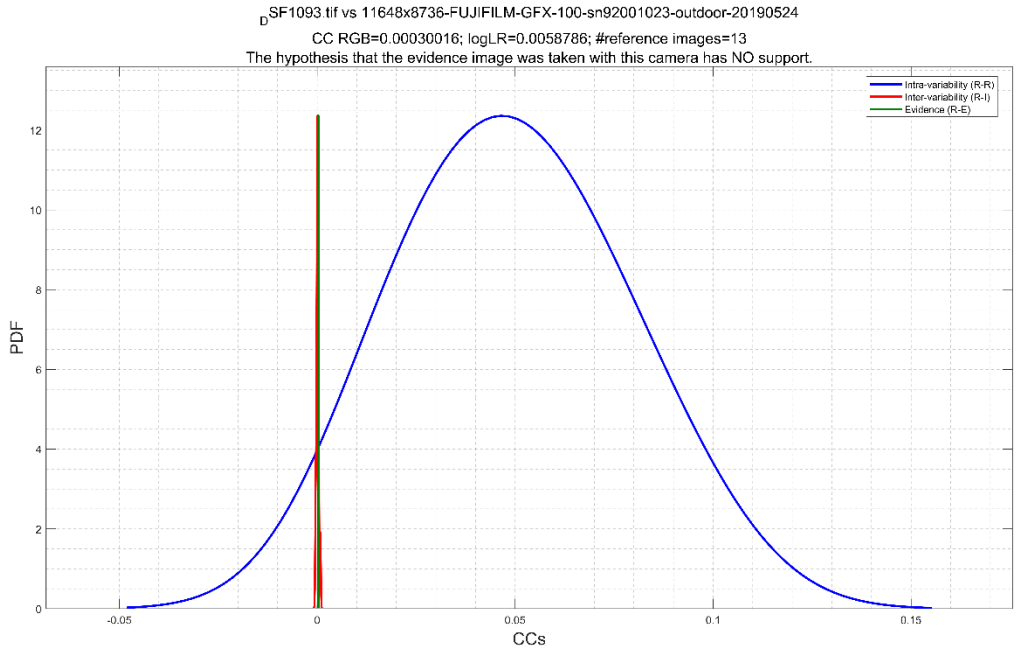
DSF1093.tif vs 11648x8736-FUJIFILM-GFX-100-sn92001023-outdoor-20190524
CC RGB=0.00030016; logLR=0.0058786; #reference images=13
The hypothesis that the evidence image was taken with this camera has NO support.
Intra-variability (R-R)
Inter-variability (R-I)
Evidence (R-E)
PDF
CCs

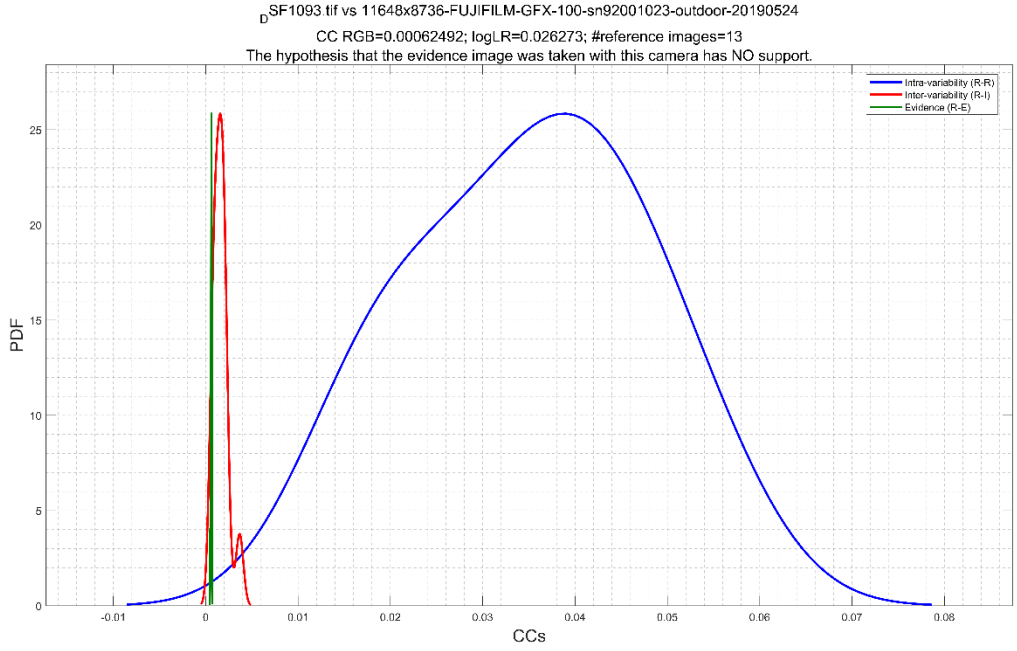
DSF1093.tif vs 11648x8736-FUJIFILM-GFX-100-sn92001023-outdoor-20190524
CC RGB=0.00062492; logLR=0.026273; #reference images=13
The hypothesis that the evidence image was taken with this camera has NO support.
Intra-variability (R-R)
Inter-variability (R-I)
Evidence (R-E)
PDF
CCs

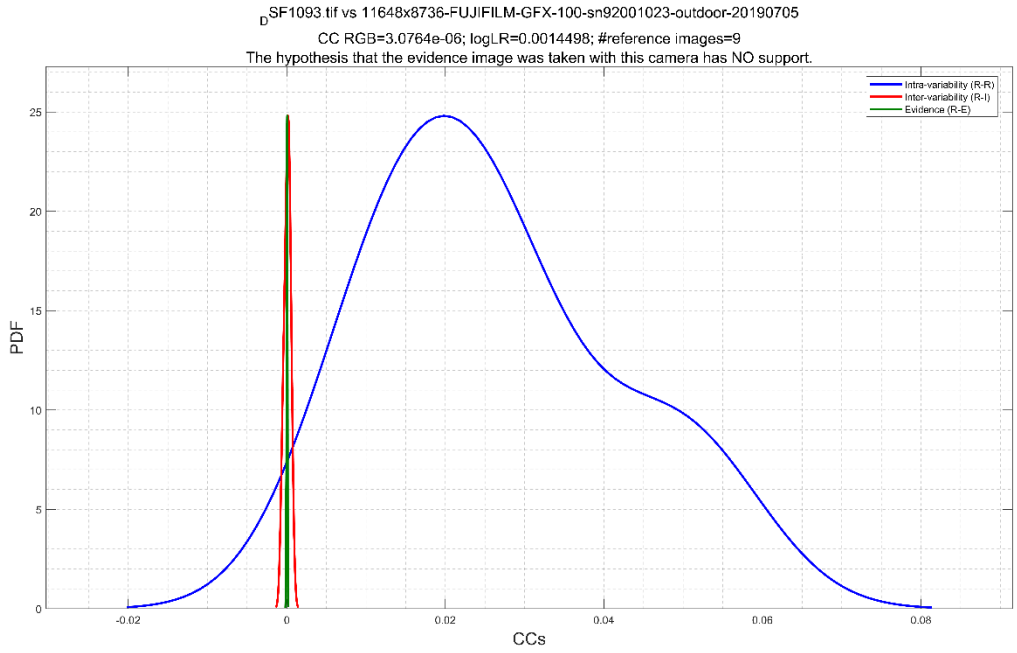
DSF1093.tif vs 11648x8736-FUJIFILM-GFX-100-sn92001023-outdoor-20190705
CC RGB=3.0764e-06; logLR=0.0014498; #reference images=9
The hypothesis that the evidence image was taken with this camera has NO support.
Intra-variability (R-R)
Inter-variability (R-I)
Evidence (R-E)
PDF
CCs

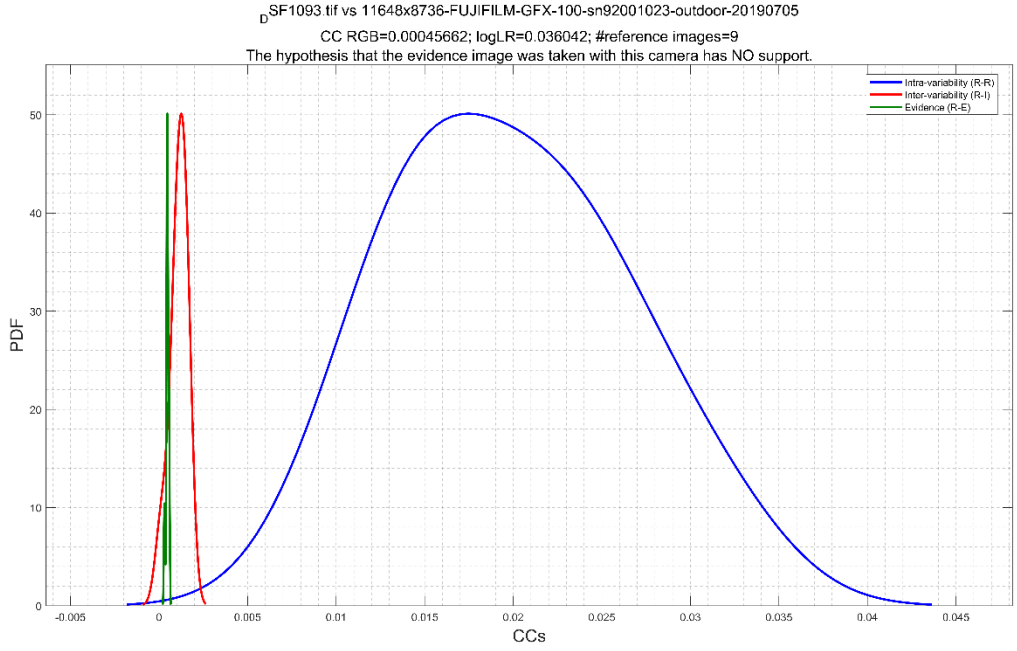
DSF1093.tif vs 11648x8736-FUJIFILM-GFX-100-sn92001023-outdoor-20190705
CC RGB=0.00045662; logLR=0.036042; #reference images=9
The hypothesis that the evidence image was taken with this camera has NO support.
Intra-variability (R-R)
Inter-variability (R-I)
Evidence (R-E)
PDF
CCs

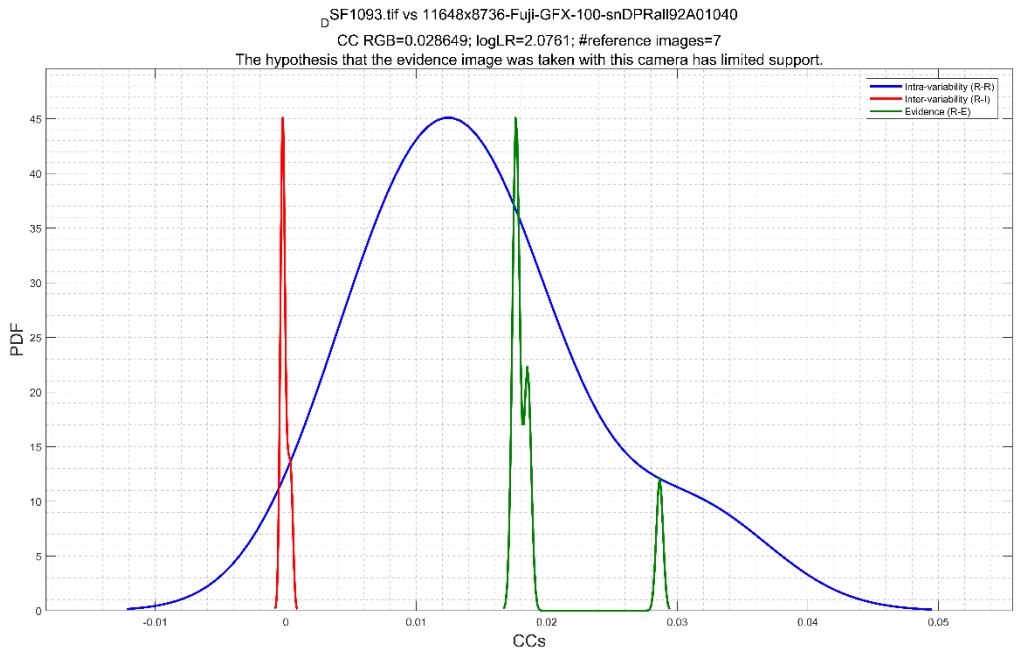
DSF1093.tif vs 11648x8736-Fuji-GFX-100-snDPRall92A01040
CC RGB=0.028649; logLR=2.0761; #reference images=7
The hypothesis that the evidence image was taken with this camera has limited support.
Intra-variability (R-R)
Inter-variability (R-I)
Evidence (R-E)
PDF
CCs

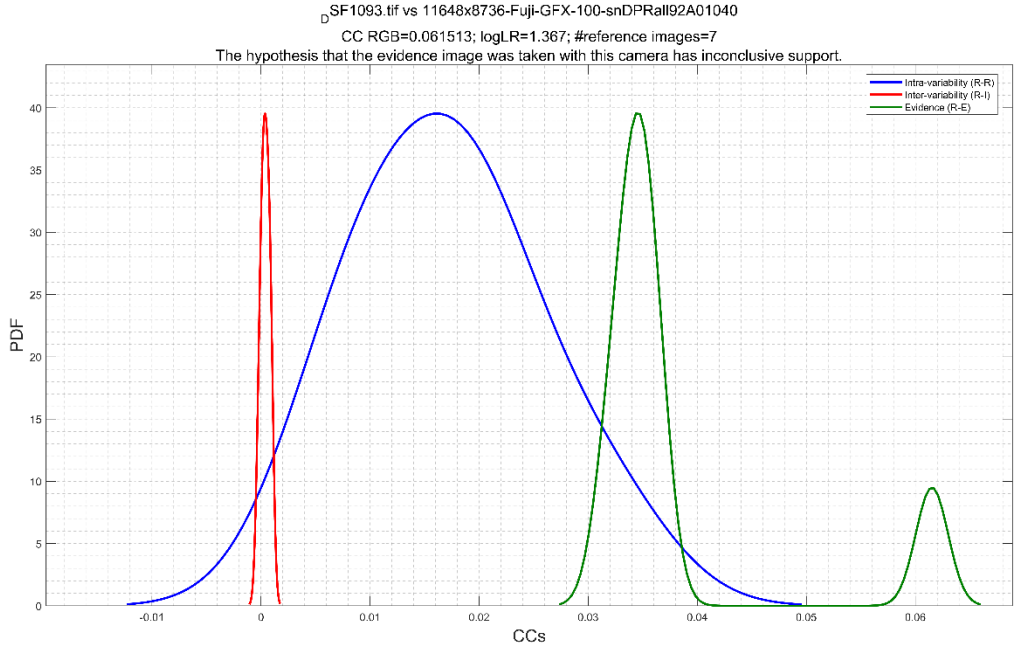
DSF1093.tif vs 11648x8736-Fuji-GFX-100-snDPRall92A01040
CC RGB=0.061513; logLR=1.367; #reference images=7
The hypothesis that the evidence image was taken with this camera has inconclusive support.
Intra-variability (R-R)
Inter-variability (R-I)
Evidence (R-E)
PDF
CCs

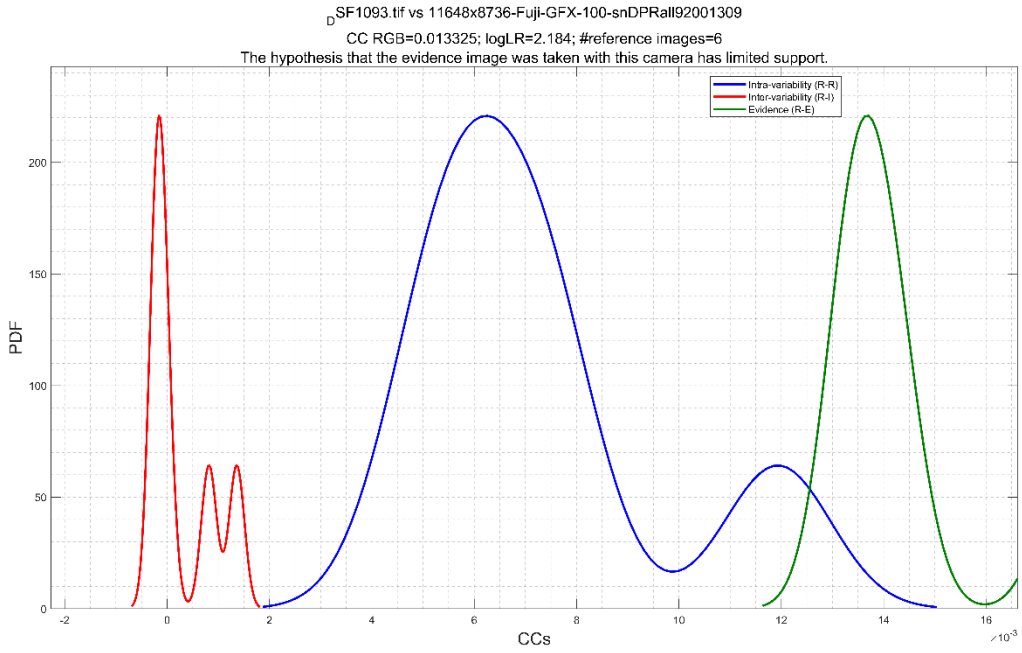
DSF1093.tif vs 11648x8736-Fuji-GFX-100-snDPRall92001309
CC RGB=0.013325; logLR=2.184; #reference images=6
The hypothesis that the evidence image was taken with this camera has limited support.
Intra-variability (R-R)
Inter-variability (R-I)
Evidence (R-E)
PDF
CCs
10^-3

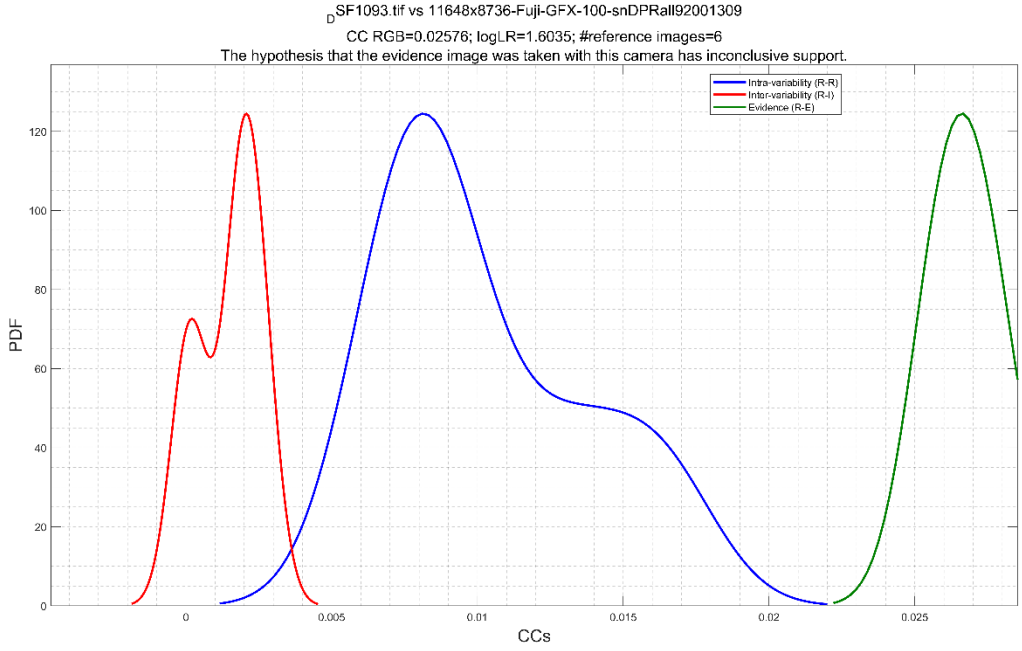
DSF1093.tif vs 11648x8736-Fuji-GFX-100-snDPRall92001309
CC RGB=0.02576; logLR=1.6035; #reference images=6
The hypothesis that the evidence image was taken with this camera has inconclusive support.
Intra-variability (R-R)
Inter-variability (R-I)
Evidence (R-E)
PDF
CCs

Hasselblad X1D II 50c

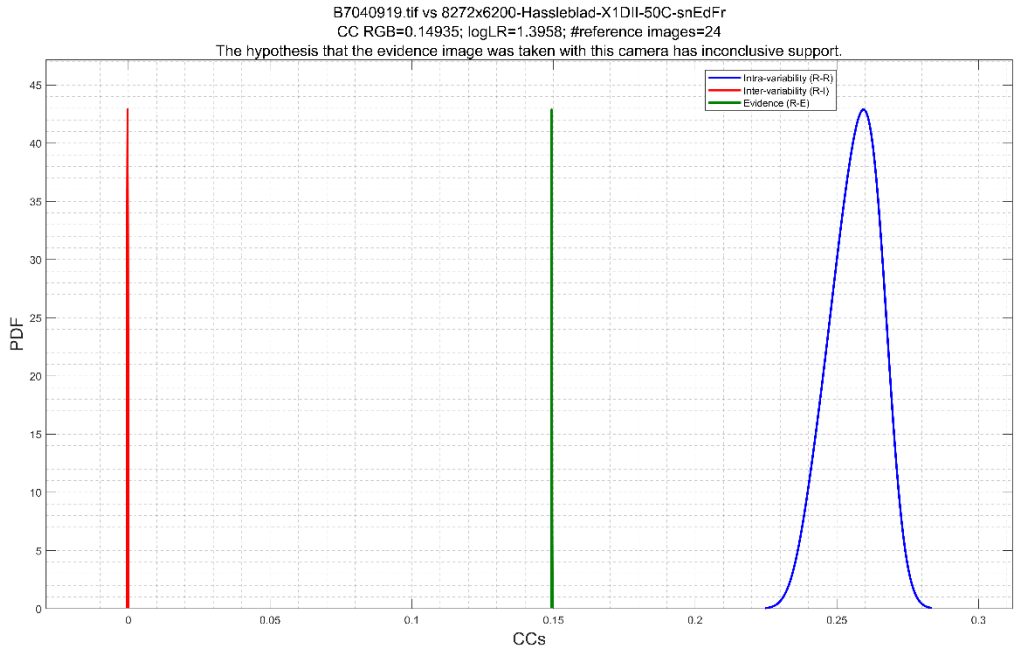

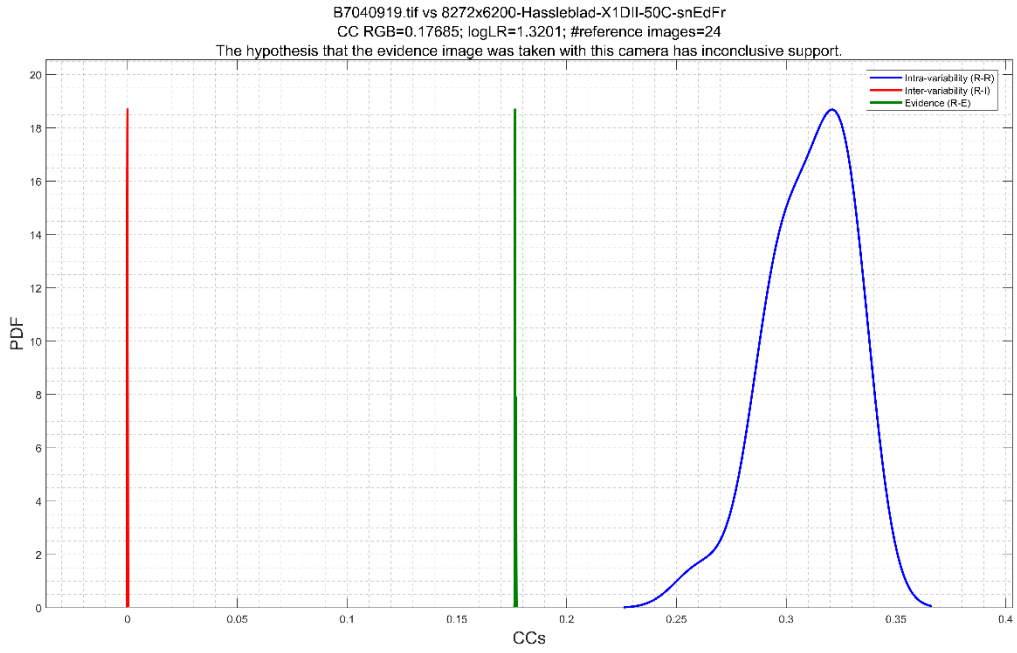

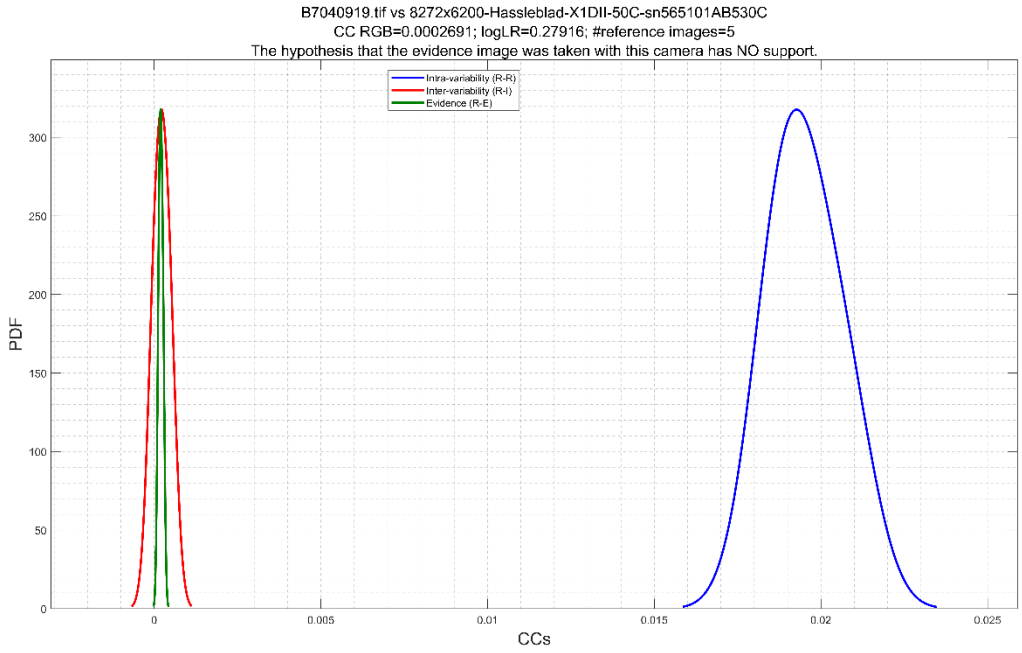
B7040919.tif vs 8272x6200-Hassleblad-X1DII-50C-sn565101AB530C
CC RGB=0.0002691; logLR=0.27916; #reference images=5
The hypothesis that the evidence image was taken with this camera has NO support.
Intra-variability (R-R)
Inter-variability (R-I)
Evidence (R-E)
PDF
CCs

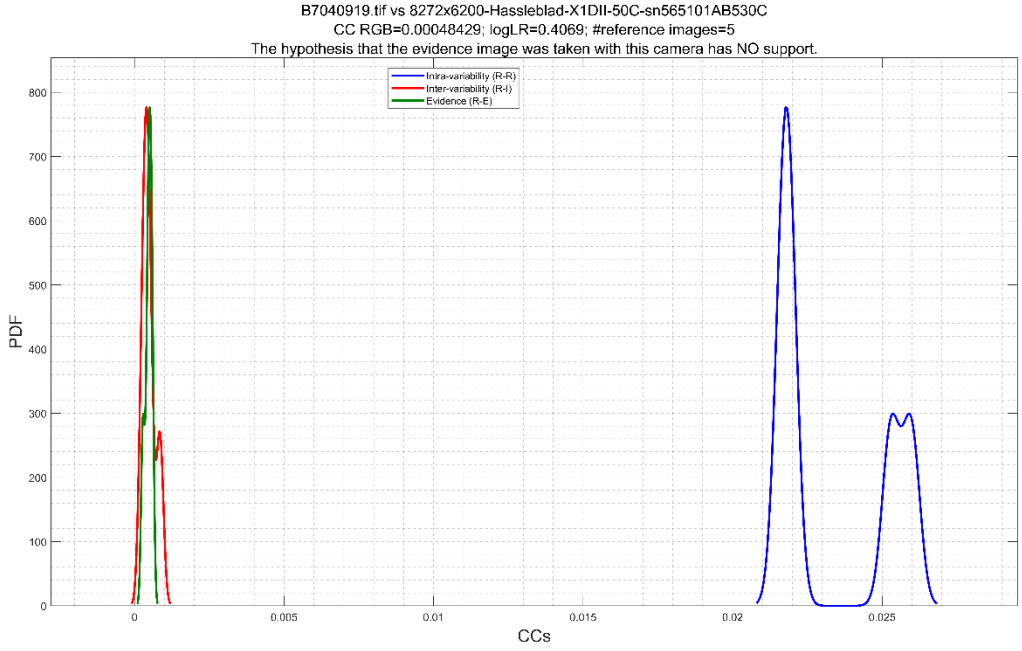
B7040919.tif vs 8272x6200-Hassleblad-X1DII-50C-sn565101AB530C
CC RGB=0.00048429; logLR=0.4069; #reference images=5
The hypothesis that the evidence image was taken with this camera has NO support.
Intra-variability (R-R)
Inter-variability (R-I)
Evidence (R-E)
PDF
CCs

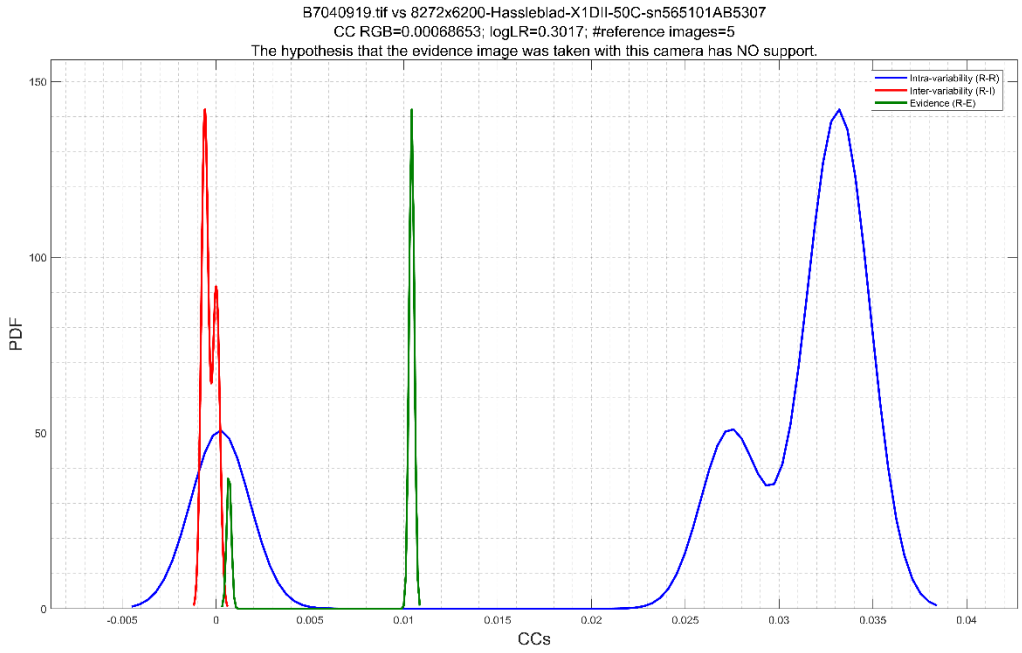
B7040919.tif vs 8272x6200-Hassleblad-X1DII-50C-sn565101AB5307
CC RGB=0.00068653; logLR=0.3017; #reference images=5
The hypothesis that the evidence image was taken with this camera has NO support.
Intra-variability (R-R)
Inter-variability (R-I)
Evidence (R-E)
PDF
CCs

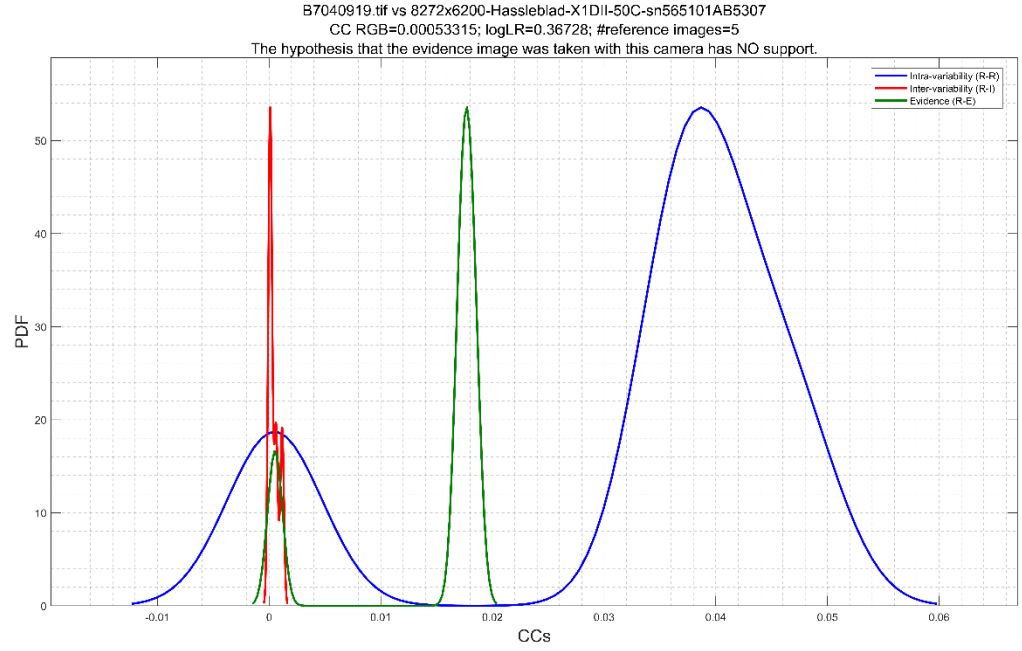
B7040919.tif vs 8272x6200-Hassleblad-X1DII-50C-sn565101AB5307
CC RGB=0.00053315; logLR=0.36728; #reference images=5
The hypothesis that the evidence image was taken with this camera has NO support.
Intra-variability (R-R)
Inter-variability (R-I)
Evidence (R-E)
PDF
CCs

Hasselblad H6D 100c

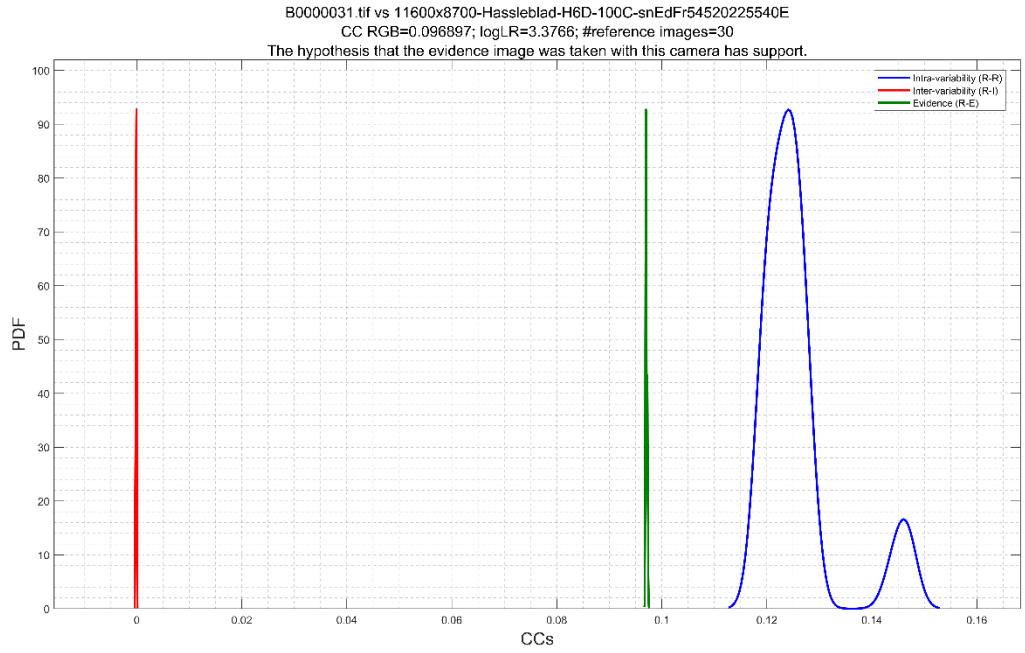

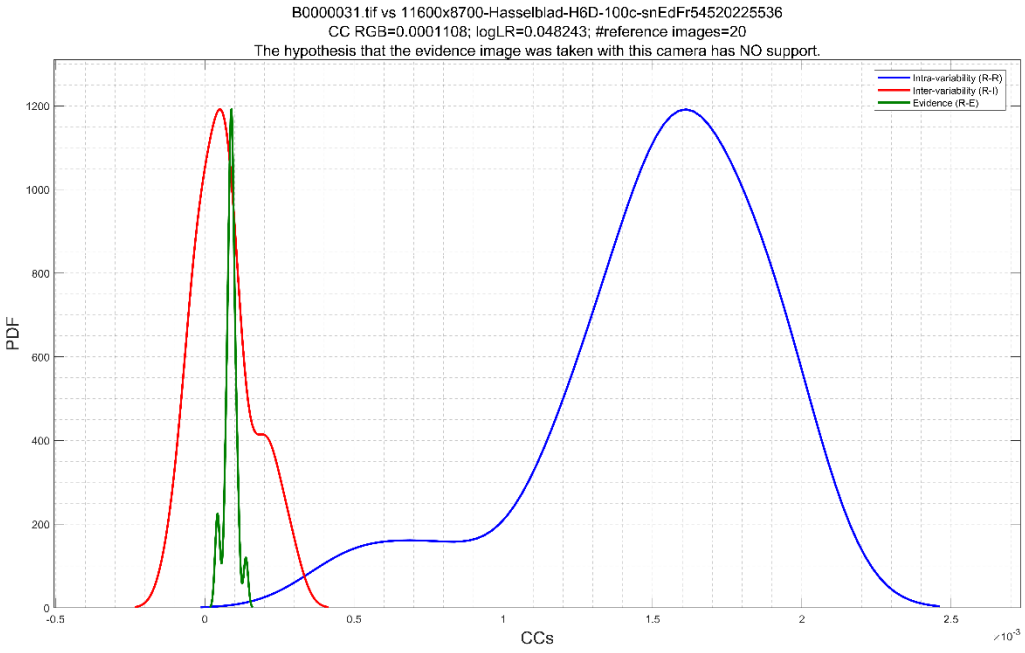

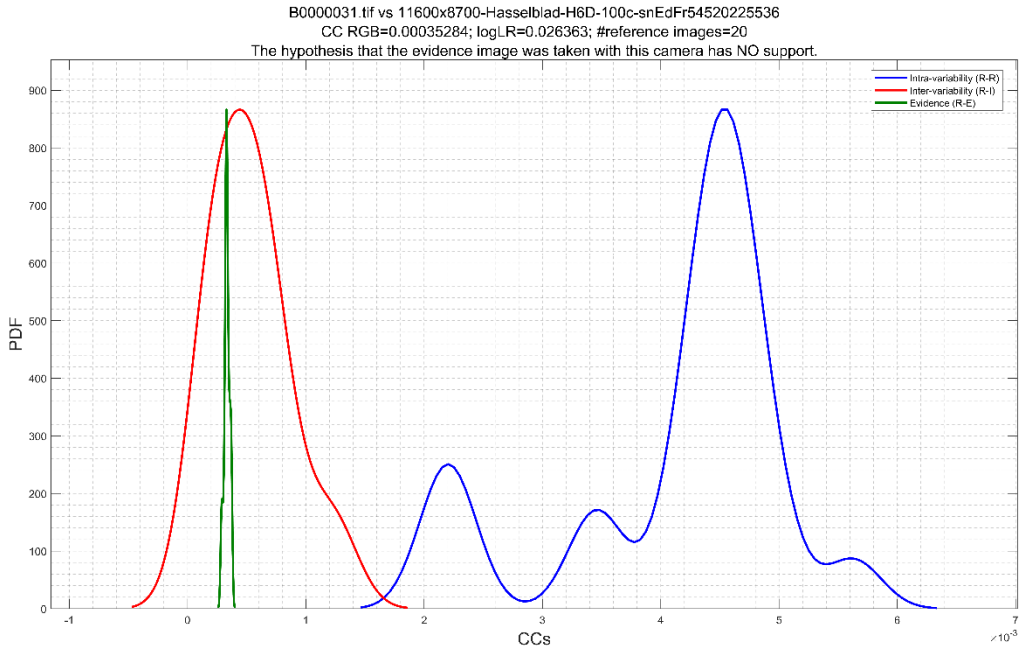
B0000031.tif vs 11600x8700-Hasselblad-H6D-100c-snEdFr54520225536
CC RGB=0.00035284; logLR=0.026363; #reference images=20
The hypothesis that the evidence image was taken with this camera has NO support.
Intra-variability (R-R)
Inter-variability (R-I)
Evidence (R-E)
PDF
CCs
10^-3

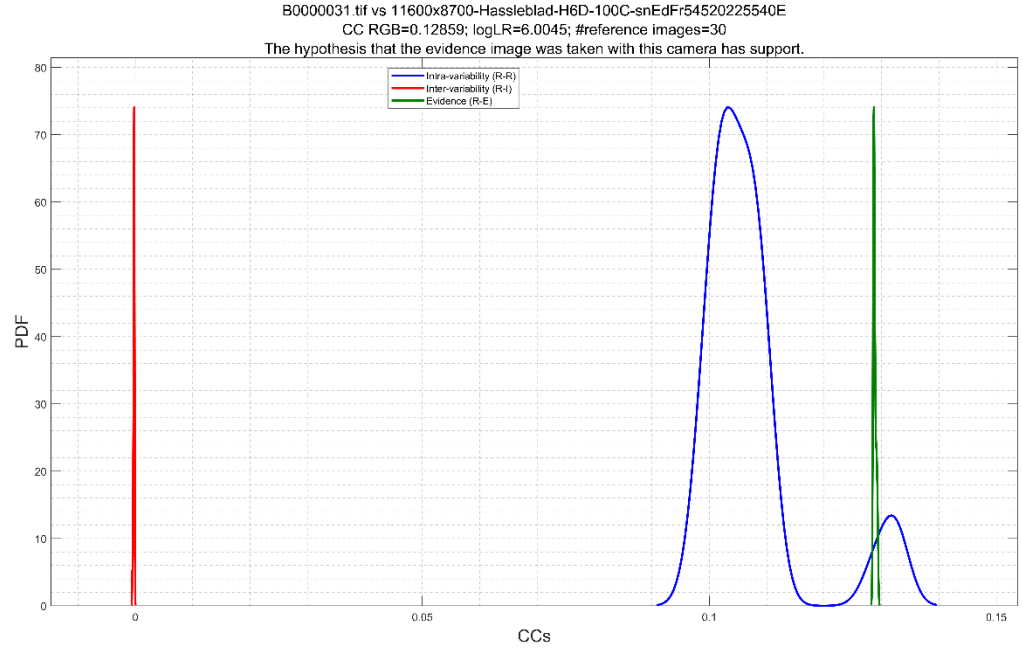
B0000031.tif vs 11600x8700-Hassleblad-H6D-100C-snEdFr545202255540E
CC RGB=0.12859; logLR=6.0045; #reference images=30
The hypothesis that the evidence image was taken with this camera has support.
Intra-variability (R-R)
Inter-variability (R-I)
Evidence (R-E)
PDF
CCs

Phase One IQ3 100 MP

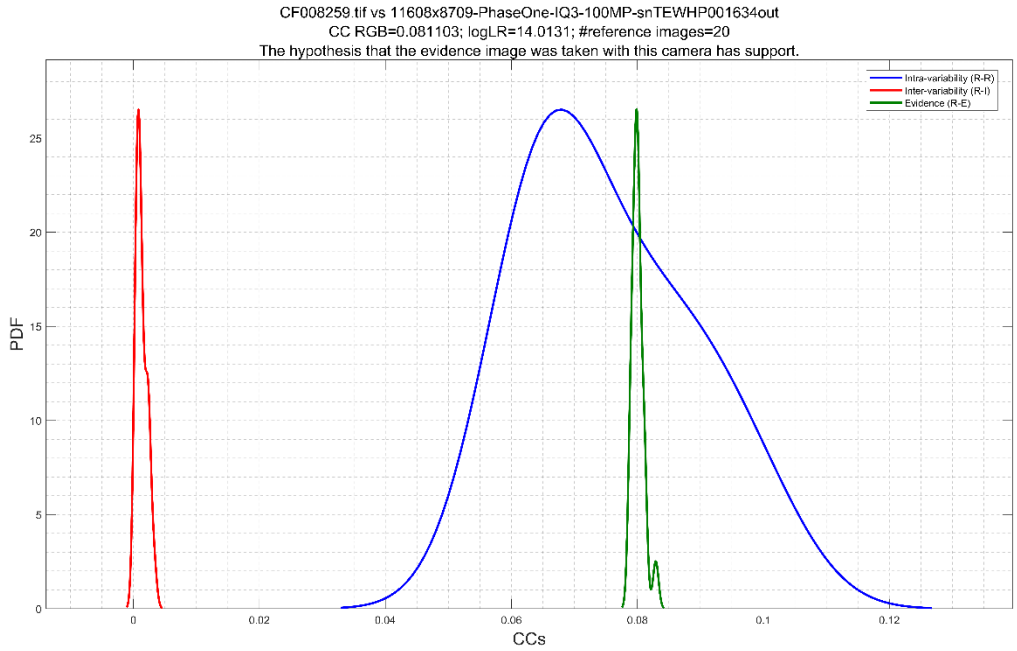

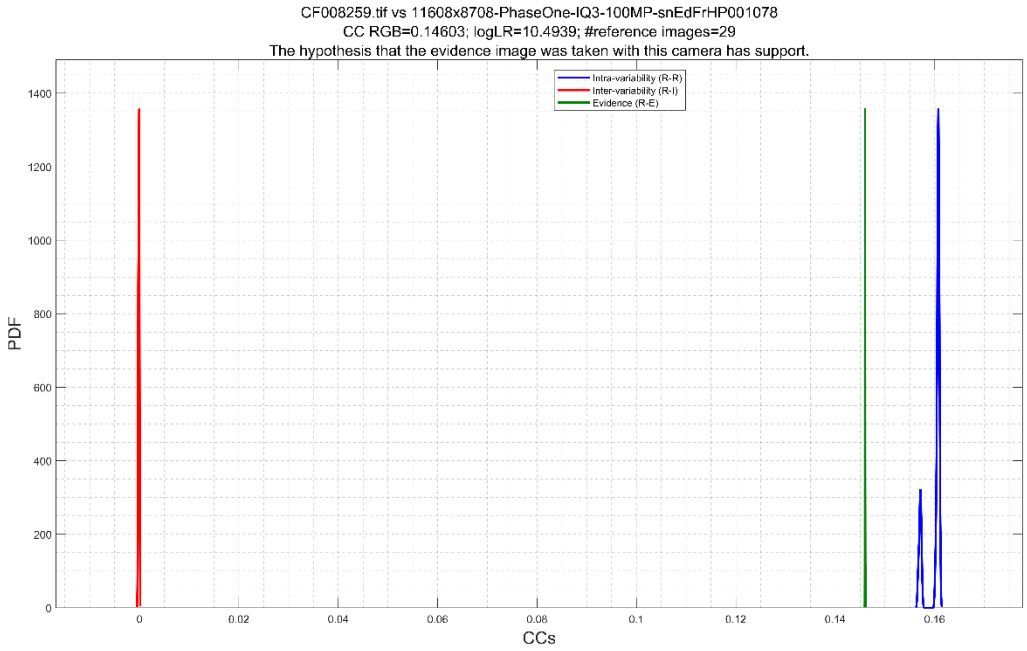

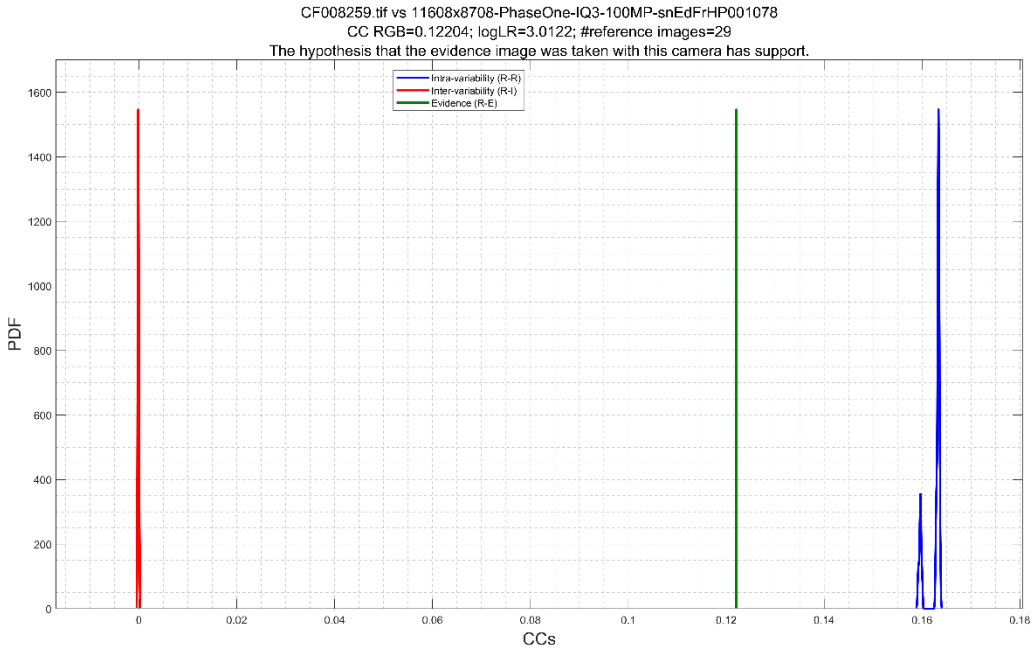
CF008259.tif vs 11608x8708-PhaseOne-IQ3-100MP-snEdFrHP001078
CC RGB=0.12204; logLR=3.0122; #reference images=29
The hypothesis that the evidence image was taken with this camera has support.
Intra-variability (R-R)
Inter-variability (R-I)
Evidence (R-E)
PDF
CCs

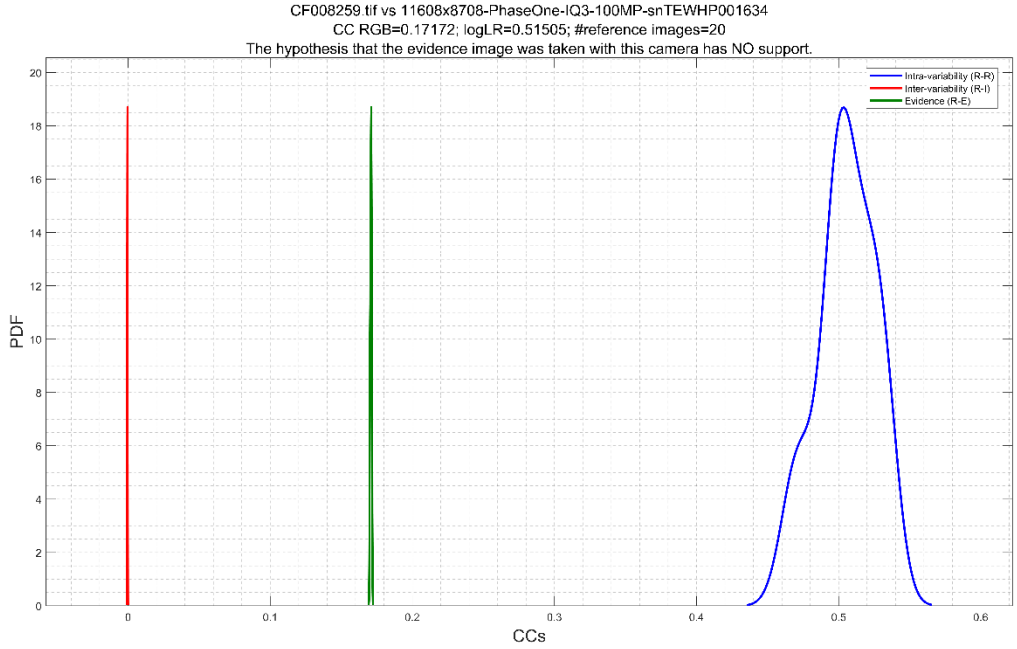
CF008259.tif vs 11608x8708-PhaseOne-IQ3-100MP-snTEWHP001634
CC RGB=0.17172; logLR=0.51505; #reference images=20
The hypothesis that the evidence image was taken with this camera has NO support.
Intra-variability (R-R)
Inter-variability (R-I)
Evidence (R-E)
PDF
CCs

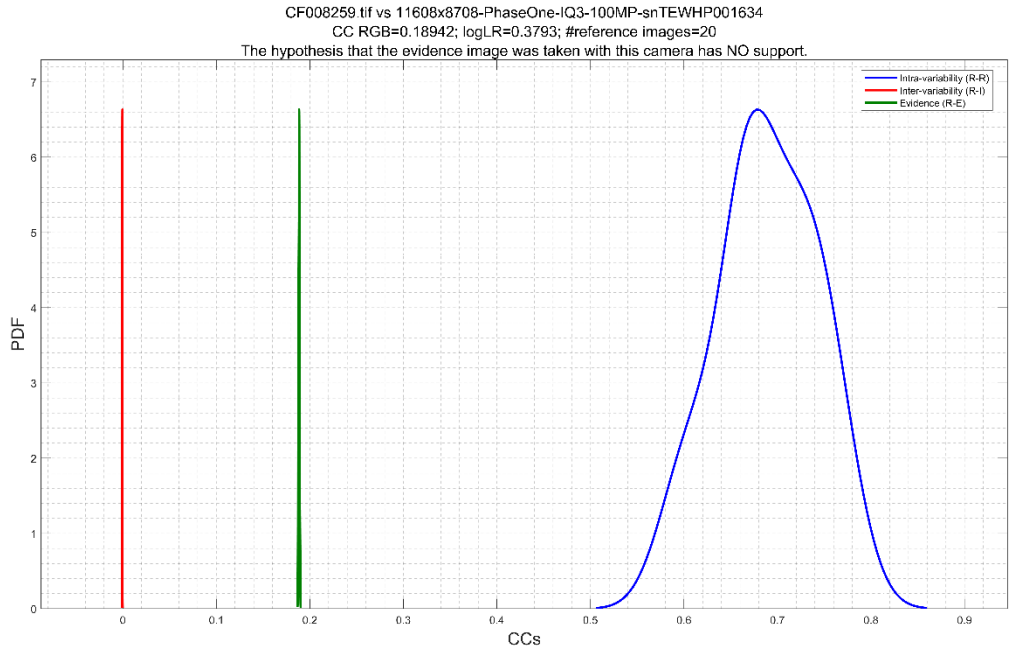
CF008259.tif vs 11608x8708-PhaseOne-IQ3-100MP-snTEWHP001634
CC RGB=0.18942; logLR=0.3793; #reference images=20
The hypothesis that the evidence image was taken with this camera has NO support.
Intra-variability (R-R)
Inter-variability (R-I)
Evidence (R-E)
PDF
CCs

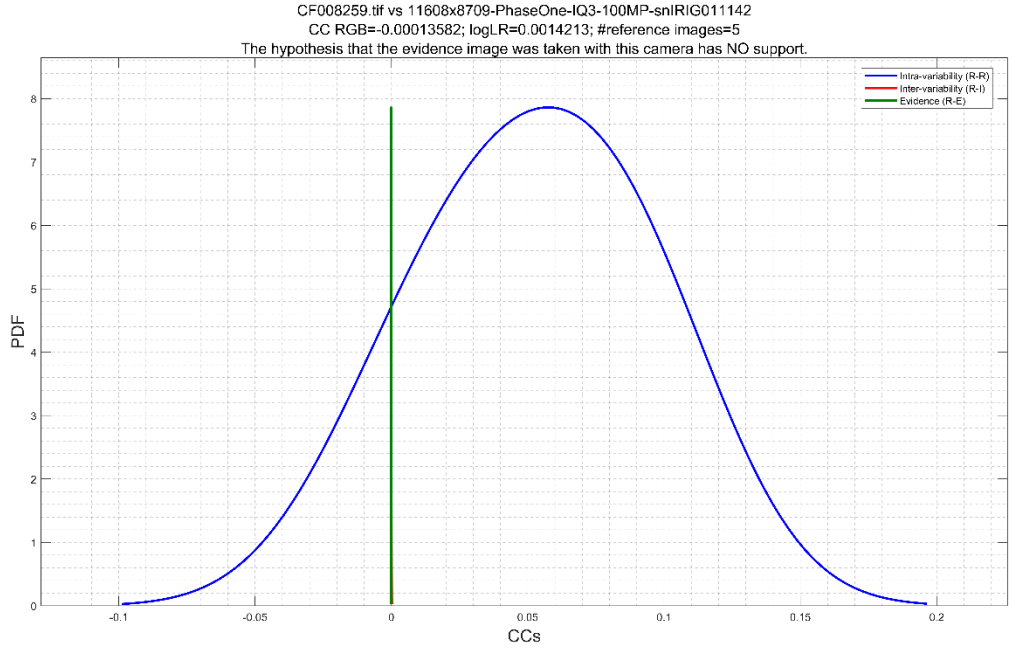
CF008259.tif vs 11608x8709-PhaseOne-IQ3-100MP-snIRIG011142
CC RGB=-0.00013582; logLR=0.0014213; #reference images=5
The hypothesis that the evidence image was taken with this camera has NO support.
Intra-variability (R-R)
Inter-variability (R-I)
Evidence (R-E)
PDF
CCs

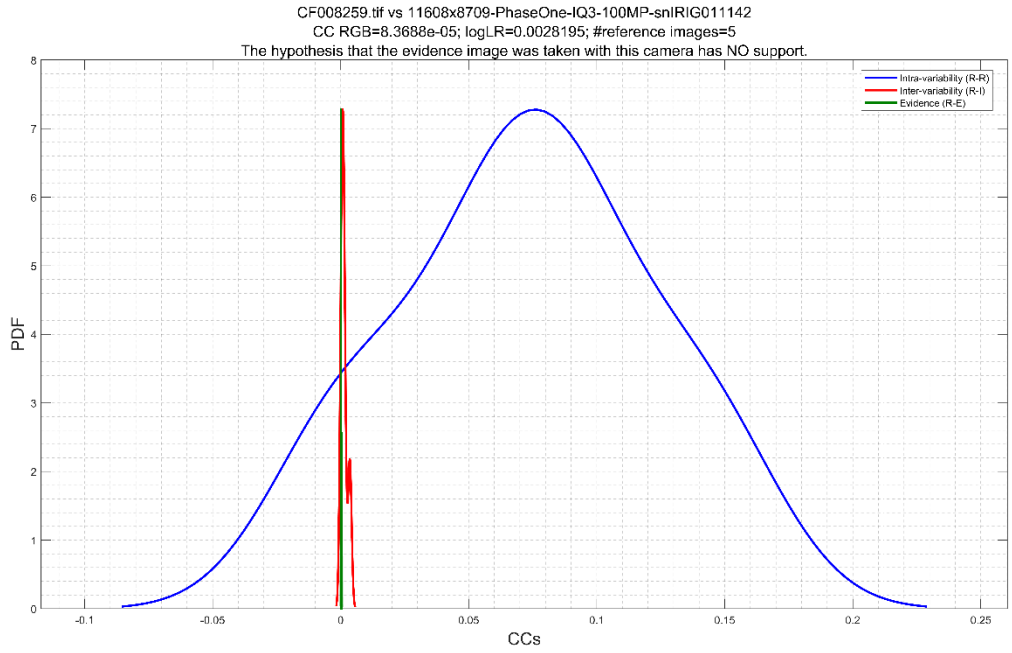
CF008259.tif vs 11608x8709-PhaseOne-IQ3-100MP-snIRIG011142
CC RGB=8.3688e-05; logLR=0.0028195; #reference images=5
The hypothesis that the evidence image was taken with this camera has NO support.
Intra-variability (R-R)
Inter-variability (R-I)
Evidence (R-E)
PDF
CCs

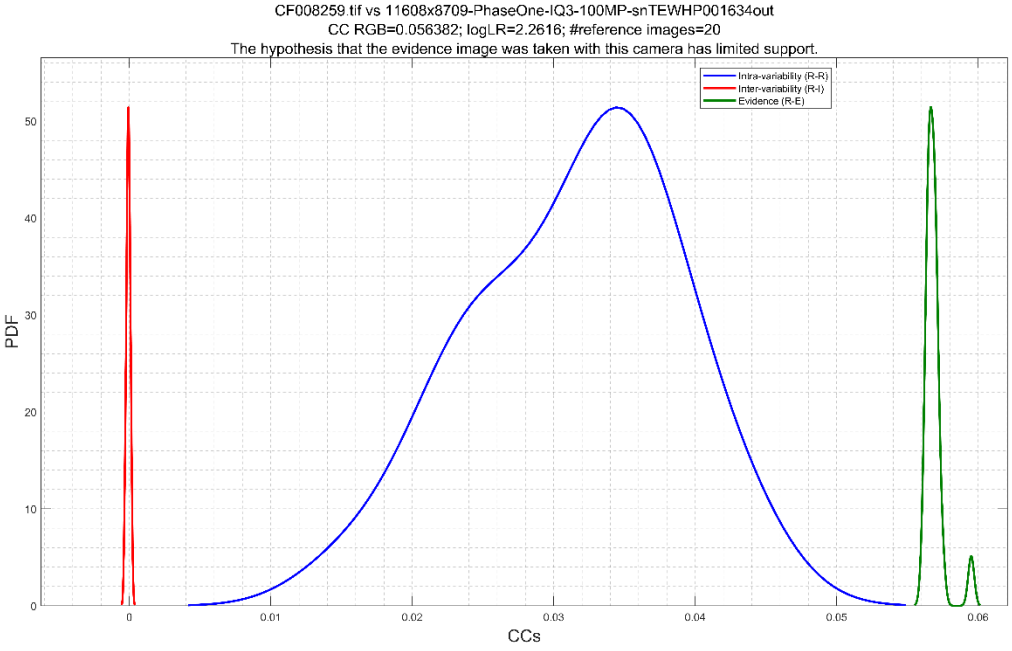
CF008259.tif vs 11608x8709-PhaseOne-IQ3-100MP-snTEWHP001634out
CC RGB=0.056382; logLR=2.2616; #reference images=20
The hypothesis that the evidence image was taken with this camera has limited support.
Intra-variability (R-R)
Inter-variability (R-I)
Evidence (R-E)
PDF
CCs

Phase One IQ4 150 MP

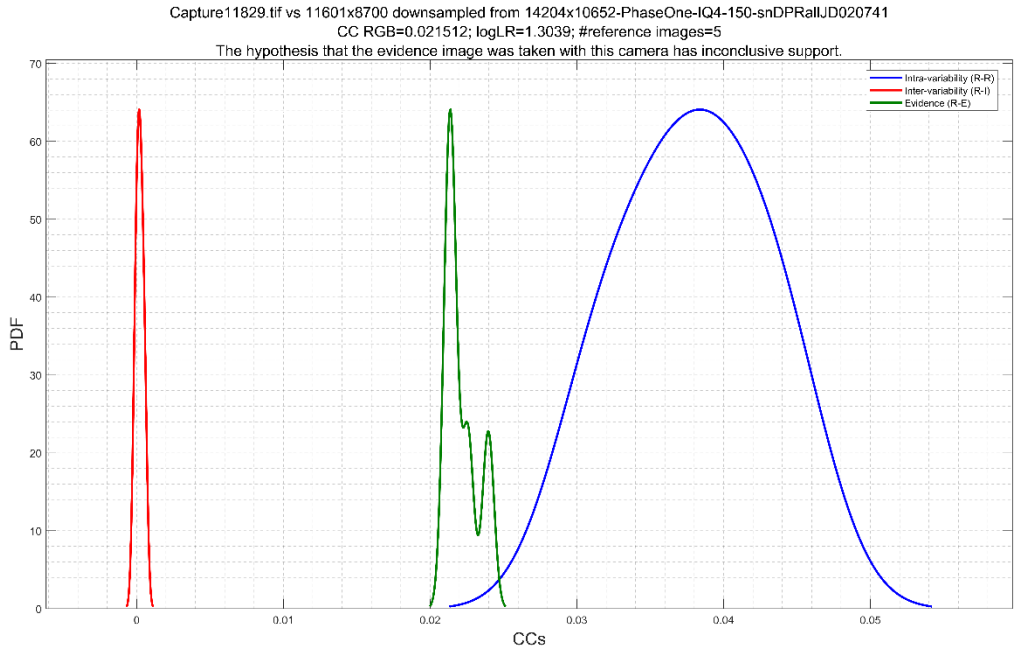

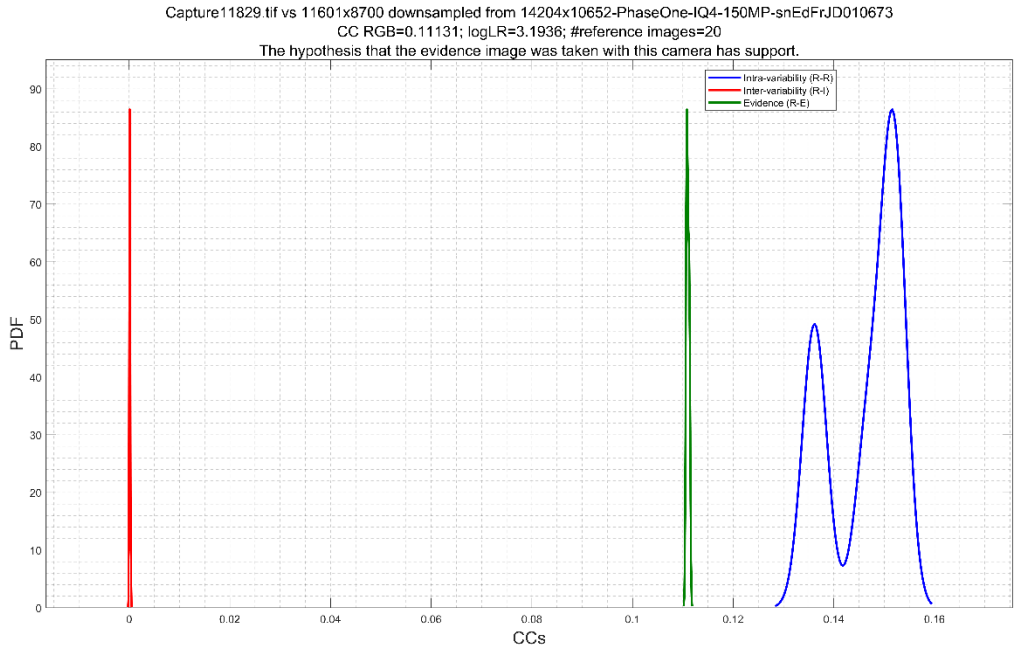

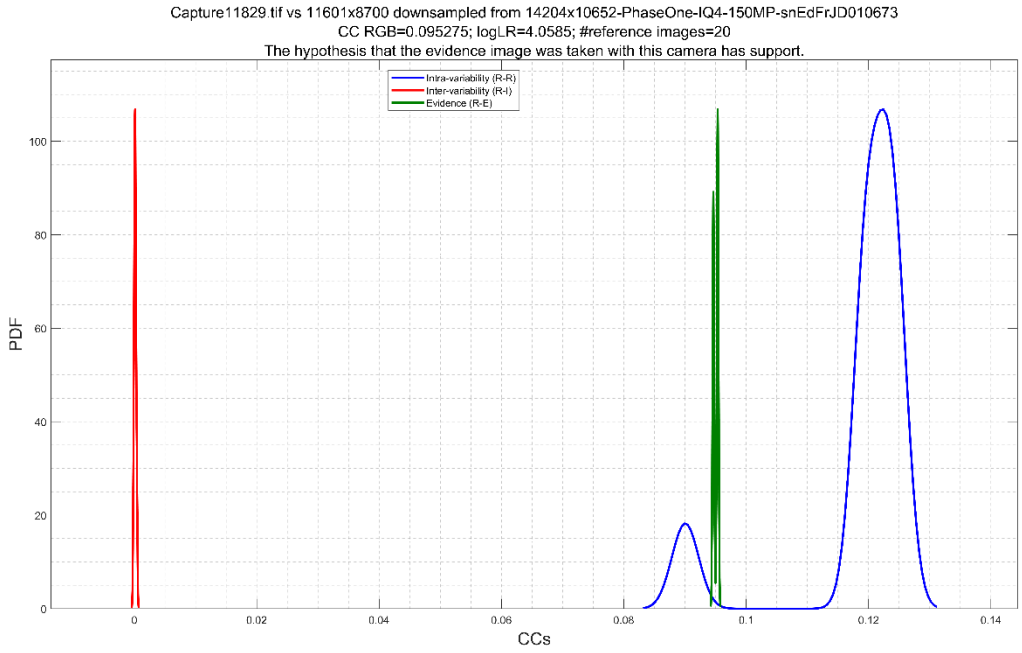
Capture11829.tif vs 11601x8700 downsampled from 14204x10652-PhaseOne-IQ4-150MP-snEdFrJD010673
CC RGB=0.095275; logLR=4.0585; #reference images=20
The hypothesis that the evidence image was taken with this camera has support.
Intra-variability (R-R)
Inter-variability (R-I)
Evidence (R-E)
PDF
CCs

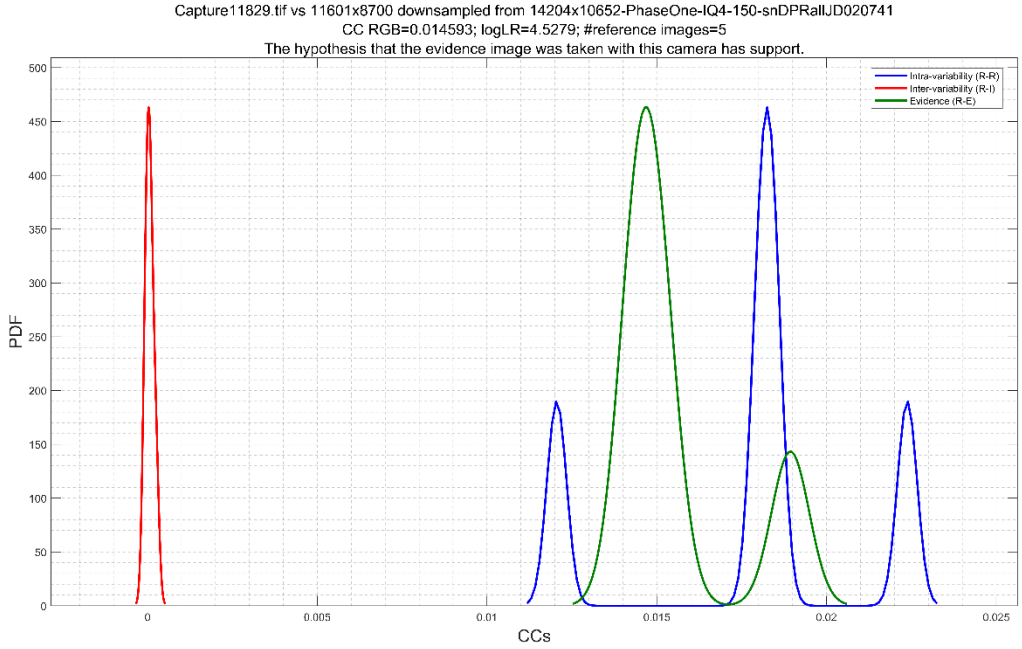
Capture11829.tif vs 11601x8700 downsampled from 14204x10652-PhaseOne-IQ4-150-snDPRallJD020741
CC RGB=0.014593; logLR=4.5279; #reference images=5
The hypothesis that the evidence image was taken with this camera has support.
Intra-variability (R-R)
Inter-variability (R-I)
Evidence (R-E)
PDF
CCs